Highlights

Comprehensive Repeatable Experiments of Ship Maneuvering in Waves

Krishnavelu Ramachandran, Abhilash Somayajula

- Full factorial experimental design across 54 test conditions provide robust benchmark data for validating numerical models of ship maneuvering in waves
- Each test condition is repeated five times to ensure repeatability and statistical robustness of the results
- Drift velocity is constant across the turn and is not affected by change in relative direction of the hull to the waves
- Comprehensive experimental investigation reveals a linear relationship between drift velocity and wave slope during turning maneuvers, indicating a different behavior from the conventional quadratic variation observed for wave drift forces and moments

Comprehensive Repeatable Experiments of Ship Maneuvering in Waves

Krishnavelu Ramachandran[a], Abhilash Somayajula[a,b,*]

[a] *Marine Autnomous Vehicles (MAV) Laboratory, Department of Ocean Engineering, IIT Madras,*

[b] *Center of Excellence for Maritime Experiments to Maritime Experience (ME2ME), IIT Madras,*

Abstract

Modern ships operate with reduced power margins to meet stringent emission regulations. This raises critical questions about their maneuverability in adverse sea conditions. Although extensive research has been conducted on ship maneuvering in waves, a fundamental limitation is the lack of systematic repeatability and rigorous uncertainty analysis, especially for experiments involving inherently transient phenomena. In turning circle maneuvers, the vessel's orientation with respect to the waves is constantly changing, making the resulting hydrodynamic forces and drift highly variable and challenging to characterize. This study addresses these gaps by presenting a comprehensive experimental investigation, comprising of 54 test cases in a full factorial design across three wave slopes (1/80, 1/60, 1/40), three wavelength-to-ship-length ratios (0.8, 1.0, 1.2), three propeller speeds, and both port and starboard 35° rudder angles. Each test condition is repeated five times, resulting in 270 test runs that enable robust statistical repeatability and detailed uncertainty quantification for these maneuvers. The analysis of the data from these runs reveal a non-intuitive trend between drift velocity and wave slope that to our knowledge has not been reported in the existing literature so far. These findings provide essential insights for the development more accurate and robust numerical models for simulating ship maneuvering in waves.

1. Introduction

The International Maritime Organization's (IMO) Energy Efficiency Design Index (EEDI) has fundamentally transformed ship design practices. This regulatory framework imposes strict limits on specific fuel consumption for new vessels, driving the maritime industry toward reduced carbon emissions. Consequently, modern ships increasingly feature lower-powered engines to achieve the mandated emission reductions. While this transition supports global decarbonization objectives and enhances fuel efficiency, it simultaneously introduces critical questions about vessel performance. Specifically, whether ships with reduced power can maintain sufficient maneuverability under realistic sea conditions?

This concern has catalyzed extensive research into ship maneuvering behavior in waves. As vessels operate with increasingly constrained power margins, phenomena such as wave-induced drift, turning circle deformation, and compromised heading control emerge as critical design and operational safety considerations. The theoretical framework for analyzing ship maneuvering in waves is built upon the development of second-order wave drift forces and moments, pioneered by Newman [1] and Maruo [2]. These hydrodynamic forces, which scale with the square of wave amplitude, generate persistent horizontal drift and play a crucial role in overall trajectory modification during ship maneuvers, especially during turning or zig-zag operations. However, the theoretical frameworks dealing with second order drift force calculation operate under the steady state

*Corresponding author

Email addresses: oe20d014@smail.iitm.ac.in (Krishnavelu Ramachandran), abhilash@iitm.ac.in (Abhilash Somayajula)

assumption and do not consider the complexity of continuous variation of wave direction and encounter frequency during the maneuver.

Ship maneuvering in waves has been of research interest since many decades with studies dating back to early 1980s [3, 4]. These early studies recommended that the inclusion of the second order wave drift forces and moments in a quasi static manner are sufficient to predict the drift distance and drift direction accurately. However, the ITTC 1981 [5] observed that the number of experimental data points available for comparison were limited. Further experimental studies were conducted by Ueno et al. [6] where the drift distance and drift direction were measured for port and starboard 35° turns over a range of λ/L ratios. In this study the wave height was kept constant and the wavelength was changed, which also resulted in a change in wave slope. It was observed that the drift distance decreased with an increase in wavelength (which also meant a decrease in wave slope). However, this study did not comment on the statistical repeatability of the tests. The study did compare simulated results based on the approach recommended by ITTC 1981 [5, 7] with the experimental results. It was however observed that the simulated results were not able to capture the experimental results accurately.

Further notable investigations were conducted by Yasukawa's group in Japan. Yasukawa et al. [8] computed the drift forces and moments using a potential theory method and compared them with experimental measurements. A simplified model based on Nomoto's formulation was proposed by Yasukawa et al. [9] for simulating the maneuvering motion of a ship in waves. This simplified model was applied to both KVLCC2 and KCS vessels undertaking a turning circle maneuver in irregular waves for different initial speeds. The drift distances and drift directions computed between the first two turns were compared with experimental measurements. The simplified model was able to capture the drift distance well but was unable to capture the drift direction accurately. Later the drift forces were incorporated into a two time scale simulation model proposed by Skejic and Faltinsen [10] and the resultant simulation results were compared with experimental measurements [11] in a steady turn with a single regular wave. In this study it was shown that simulation captured the surge speed reduction well but the variation in sway velocity and yaw rate were not captured accurately.

Some of the other experimental studies include Klamo and Lin [12], which conducted extensive experiments of turning circles of a ship in regular waves and concluded that for a slow ship, small rudder angle and steep wave can significantly impact the ability of the ship to perform the maneuver. The study observed that the drift direction varied significantly across the runs and its trend could not be understood accurately. While the study did not analyze the drift distance in detail, it reported that the time to complete one turn and the steady diameter increased with an increase in wave slope. This was one of the few studies that reported uncertainty in the experimental results and emphasized the need for more experimental data with repeatability.

More recent studies by Kim et al. [13, 14] reported the drift behavior of the KVLCC2 and KCS vessels in regular waves during turning maneuvers. For KVLCC2, systematic variations of drift distance and drift direction with wave slope and wavelength were presented, while the later study extended the analysis to KCS and considered obstacle-avoidance performance in waves. These studies are widely referenced in the field, but they did not include statistical repeatability or quantify uncertainty. In addition, their focus was limited to drift distance and direction, without addressing the behavior of drift velocity.

Sanada et al. [15] reported turning circle and zig-zag maneuvers of the ONR Tumblehome vessel in calm water and regular waves and compared them with KVLCC2 and S175 container ship data from previous studies. This study reported uncertainty by repeating some of the maneuvers twice. The drift distance and drift direction variations with speed, rudder angle (port and starboard) and wave length were reported. However, the variation with wave slope was not investigated.

Some of the notable studies from Europe include Moctar and Sprenger [16, 17]. These studies reported the effect of waves on turning circle maneuvers of KVLCC2 and DTC (Duisberg Container Ship) models. The main interest of these studies was to develop numerical models that could accurately predict the trajectories of the ships in waves. The drift distance investigation was not conducted in these studies.

Despite the extensive research conducted on ship maneuvering in waves, several critical gaps remain that limit the understanding of the complex interactions between wave conditions and ship performance. A key limitation across most studies is the lack of systematic repeatability tests to quantify experimental uncertainties. For instance, Kim et al. [13, 14] and others provided valuable datasets on drift distance and drift direction for the KVLCC2 and KCS, but, like most prior studies, did not report repeatability or uncertainty. Klamo and Lin [12] remain one of the few to explicitly address this issue, highlighting the importance of incorporating uncertainty analysis in future experimental campaigns.

Furthermore, the experimental test matrices in existing studies have typically considered varying only one or two parameters simultaneously. This approach, while necessary to manage experimental complexity, fails to capture the full parameter space that influences ship maneuvering behavior in waves. Most studies have not systematically explored the combined effects of wave slope, wavelength-to-ship-length ratio, ship speed, and rudder angle (for both port and starboard turns) in a comprehensive manner. This limitation stems from the geometric growth in test cases required for a full factorial experimental design.

The current experimental investigation addresses these research gaps through a systematic and comprehensive approach. The study implements a full experimental design encompassing three different wave slopes, three wavelength-to-ship-length ratios, three ship speeds, and two rudder angles (-35° and +35°), resulting in 54 test cases. To ensure statistical reliability and to quantify experimental uncertainties, each test condition is repeated five times, providing robust data for uncertainty analysis and trend identification. This extensive dataset of 270 individual turning circle tests provides the foundation for a detailed analysis of various drift parameters that have not previously been reported in the literature.

Beyond providing benchmark experimental data, this study aims to advance the understanding of the underlying physics by analyzing trajectory data to explain the observed trends in drift parameters. The comprehensive repeatable experiments will enable the development of more accurate numerical models [18, 19, 20] and provide insights into the fundamental mechanisms governing ship maneuvering behavior in waves. The analysis of the data reveals a non-intuitive trend between the drift velocity and the wave slope, which to our knowledge have not been reported by the recent classical studies. These findings underline the need to revisit existing theoretical frameworks and develop newer numerical models for maneuvering in waves.

2. Experiment setup

2.1. Hull

In this study the benchmark KVLCC2 hull is used to study the effect of waves on the drift experienced by a ship in waves. A $1:110$ scaled model of the vessel is outfitted with a brushless DC (BLDC) motor that drives the propeller and a stepper motor that drives the rudder. The particulars of the vessel are listed in Table 1 and the body plan for the full scale vessel is shown in Figure 1a. The GM has been estimated through inclining experiment. The vessel is ballasted to achieve the desired displacement at an even keel. The roll natural period is determined from a roll decay test.

Table 1: KVLCC2 vessel particulars

Sl. No.	Parameter	Full Scale	Model Scale
1	Length (m)	320.00	2.909
2	Breadth (m)	58.00	0.527
3	Depth (m)	28.00	0.255
4	Draft (m)	20.80	0.189
5	Block coefficient	0.809	0.809
6	Displacement (m^3)	312622	0.2348
7	Froude Number F_n	0.1420	0.1420
8	Design speed (m/s)	7.97 (15.5 kts)	0.759

Sl. No.	Parameter	Full Scale	Model Scale
9	GM (m)	4.03	0.037
10	LCG (from midship) (m)	11.13	0.101
11	Roll natural period (s)	19.31	1.84

2.2. Propeller and Rudder

This experiment utilizes a different propeller than the one specified by the SIMMAN workshop. The original benchmark propeller is swapped by the propeller of the ONR Tumblehome to enable faster acceleration of the vessel and to maintain a higher slipstream velocity across the rudder. A comparison of the propeller open water thrust characteristics of the benchmark propeller and the propeller utilized in this study is shown in Figure 2. It can be seen that the thrust coefficient of the propeller utilized in this study is significantly higher than the benchmark propeller and allows for the vessel to accelerate to steady state faster.

In order to keep the vessel maneuverable in a test basin of size 30 m $\times$ 30 m, the vessel is outfitted with a horn type Becker rudder (flap rudder) instead of the regular horn rudder. The Becker rudder as seen in Figure 3 allows for the flap portion of the rudder to experience a larger angle of attack and thus generate a larger rudder force. Here the flap rotates by twice as much as the angle of the rudder. Thus, if the rudder angle of 35° is commanded, the flap angle is 70° with respect to the ship centerline. This makes the rudder more effective as compared to the traditional rudder and is particularly useful in maneuvering vessels in constricted spaces. One of the challenges in the conduct of the proposed experiments is that the vessel will come close to the beach towards the end of a run and there is very little space to maneuver the vessel out to safety while avoiding a collision with the basin walls. The Becker rudder makes this constricted space maneuver possible. In addition, the Becker rudder will result in lower radius turns as compared to the traditional horn rudder. This allows for the turning circles to be tighter and allow for reliable capture of multiple drifting turning circles before the vessel reaches the banks of the wave basin.

The model scale particulars of the propeller and rudder used in this study and the benchmark propeller and rudder are compared in Table 2.

Table 2: Model scale propeller and rudder particulars

Sl. No.	Parameter	Benchmark	This study
1	Propeller diameter (m)	0.0896	0.1065
2	Number of blades	4	4
3	Rotation	Right handed	Left handed
4	Rudder type	Horn	Horn Becker

2.3. Sensors

The model is equipped with an Inertial Measurement Unit (IMU) that measures the linear accelerations, angular rates and magnetic field. The IMU also estimates the attitude of the vessel using an Extended Kalman Filter (EKF). The IMU is mounted on the deck at the midship section of the vessel. The IMU publishes data at 100 Hz. In order to locate the position of the vessel in the wave basin, an UWB (Ultra Wideband) rover tag is attached to the vessel at the midship. Four anchor tags are located at the corners of a square encompassing the wave basin. The anchor tags communicate with the rover tag on the vehicle using UWB communication. The time of arrival of the signal from the anchor tags is used to tri-laterate the position of the vessel. The position estimates from UWB are published at 5 Hz. Encoders connected to the motor shafts are used to measure the propeller speed and the rudder angle. The encoder data is published at 10 Hz rate. The data is published through Robot Operating System (ROS) 2 middleware and is stored in a ROS2 bag file on the on-board Raspberry Pi 4 microprocessor board. The wave data is captured through a resistance wave probe attached to the bridge of the basin at a distance of approximately 10 m from the wave maker and its voltage is also recorded to the collected ROS2 bag.

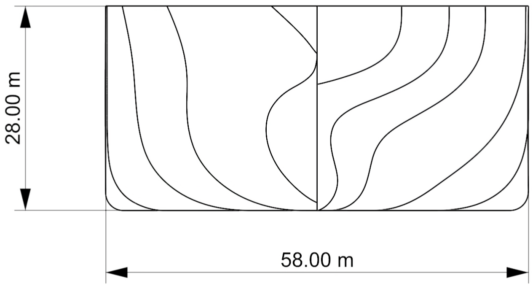

(a) KVLCC2 full scale body plan

(b) KVLCC2 model

Figure 1: KVLCC2 full scale body plan and model used in this study.

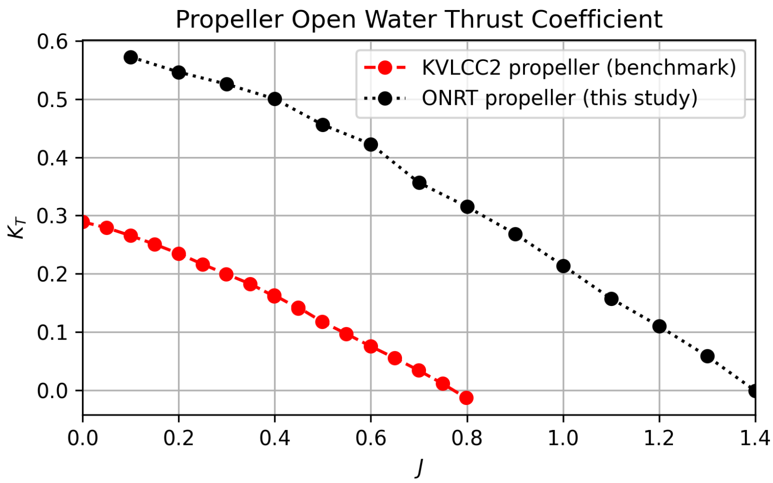

Figure 2: Propeller open water thrust coefficient

Figure 3: Rudder and propeller outfitted on the vessel

2.4. Conduct of the experiment

The global coordinate system (GCS) coincides with the UWB frame of reference. The x-axis is oriented along the north direction and the y-axis is oriented along the east direction. One corner of the wave basin is at the origin and the opposite corner of the wave basin has coordinates $(30\ m, 30\ m)$. The side along the x-axis has a 52 paddle wavemaker that is used to generate unidirectional regular waves propagating along the y-axis. The opposite end of the wave basin from the wave maker has a wave beach that allows the generated waves to break and dissipate. The wave basin has a water depth of 3 m.

Each run is started off with the vessel's bow facing towards the wave maker. The vessel is initialized with a rudder angle of $\pm 35^\circ$ ($+35^\circ$ for starboard turn and -35° for port turn) and specified propeller RPM (600 or 700 or 800). The vessel is allowed to execute two turns in calm water before the wave maker is turned on to generate the waves. The data is collected for about 400 seconds since the initial propeller and rudder commands are given. In cases where the vessel drifts too close to the wave beach, the control of the vehicle is taken over by the operator and the recording is stopped. During the post-processing phase, the data is filtered to remove the noise in the data and clipped to remove the portions where the vessel is being controlled by the operator. The vessel experiencing waves during one of the runs in the wave basin is shown in Figure 4.

Figure 4: Vessel experiencing waves in the wave basin

3. Results and Discussion

3.1. Sample Case

The results for the case of $\lambda/L = 1.0$, $H/\lambda = 1/60$, propeller speed of 700 RPM and rudder angle of $+35^\circ$ are shown in Figure 5 and Figure 6.

From Figure 5a it can be seen that the vessel starts with an orientation along the negative y-axis and settles into a steady turn over the course of two turning circles. At the end of the second turn, the wavemaker starts generating the regular waves that propagate along the y-axis. By the end of the third turn, the vessel

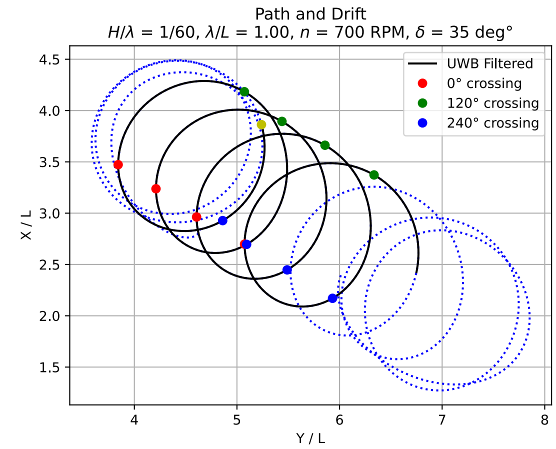

(a) Full drift path

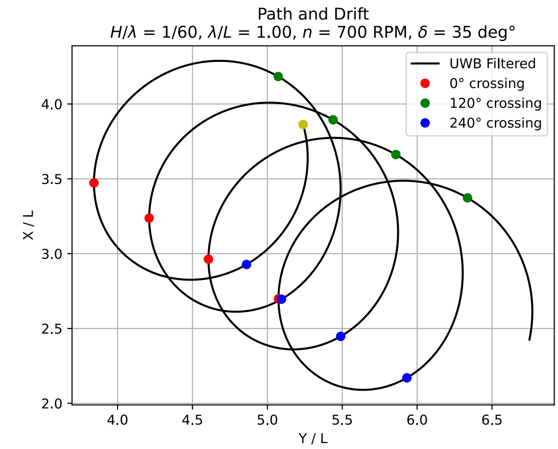

(b) Steady drift path

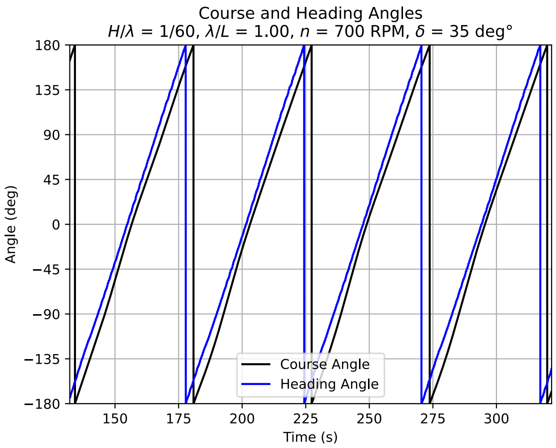

(c) Course and heading angles

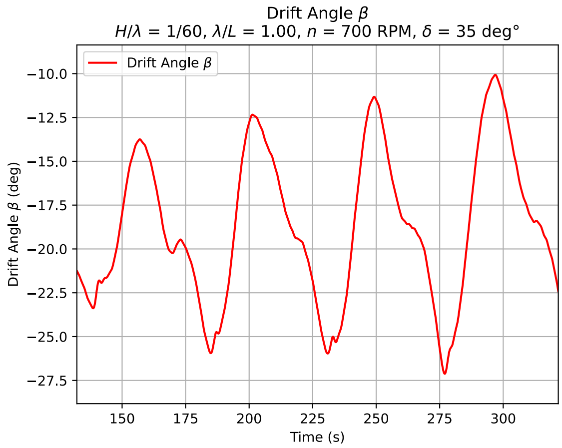

(d) Drift angle

Figure 5: Drift path, course, heading and drift angles for $\lambda/L = 1.0$, $H/\lambda = 1/60$, propeller speed of 700 RPM and rudder angle of $+35^{\circ}$

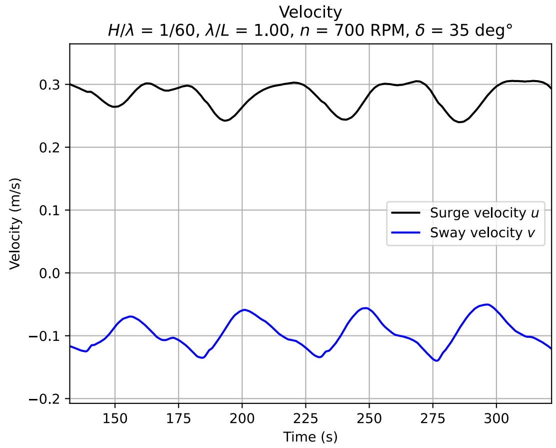

(a) Model scale velocity in BCS

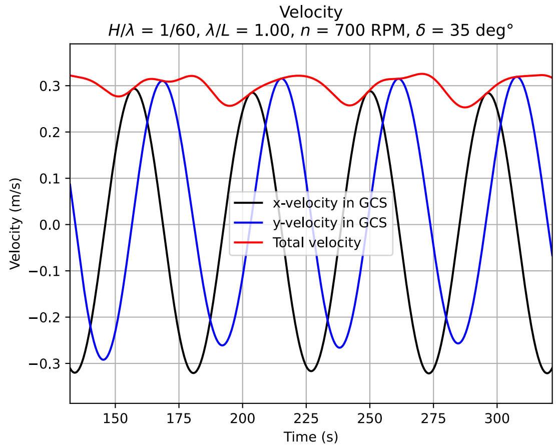

(b) Model scale velocity in GCS

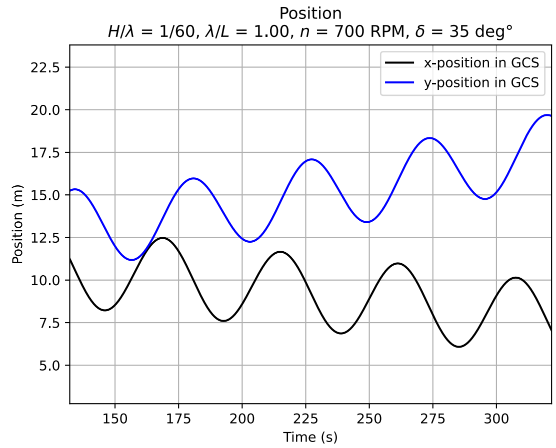

(c) Model scale position in GCS

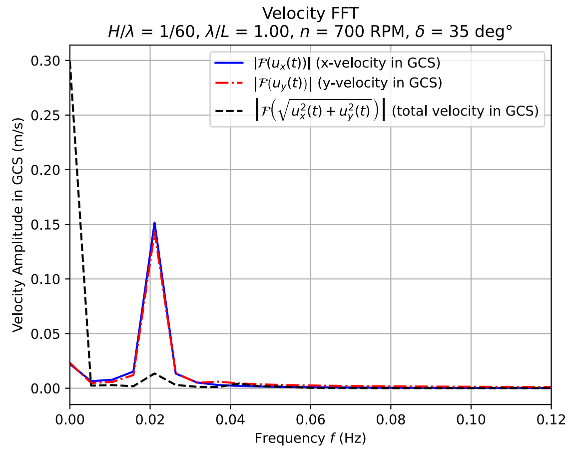

(d) Model scale velocity FFT

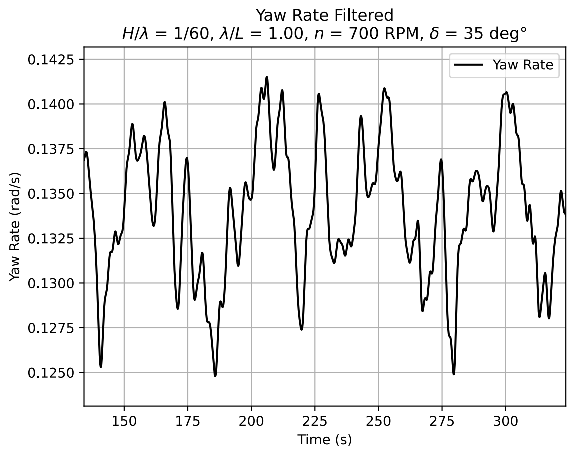

(e) Model scale yaw rate

Figure 6: Velocities, positions and yaw rate for $\lambda/L = 1.0$, $H/\lambda = 1/60$, propeller speed of 700 RPM and rudder angle of $+35°$

would be encountering steady waves. The vessel is allowed to complete as many turns as possible before the vessel drifts too close to the wave beach. In order to consider only steady wave conditions without the effect of the beach, turns 4 through 7 are used for analysis. In higher wave slopes, the vessel would experience a larger drift and reach the beach closer and fewer runs would be available for analysis. The extracted steady drift path for analysis is shown in Figure 5b.

The course and heading angles of the vessel over the steady drift path are shown in Figure 5c. In a calm water steady turn, the difference between the course and heading angles will be constant and is defined as the drift angle $\beta = (\psi - \chi)$. The drift angle of the vessel over the steady drift path is shown in Figure 5d. It can be seen that the drift angle oscillates around a mean value. When the heading and course are close to 0° (waves are incident from port side), the magnitude of the drift angle is the smallest as the drift forces from the waves are in the opposite direction of the sway velocity. When the heading and course are close to 180° (waves are incident from starboard side), the magnitude of the drift angle is the largest as the drift forces from the waves are in the same direction as the sway velocity. When the heading and course angle are 90° (following waves) or -90° (head waves), the magnitude of the drift angle is close to the mean value observed during the calm water steady turn.

The filtered surge and sway velocities of the model are shown in Figure 6a and the corresponding velocities in the global frame are shown in Figure 6b. It can be seen that the total velocity and the surge velocity experience a dip when the vessel is oriented almost head on towards the waves (around -90° course angle).

It can be observed from Figure 6b that the mean values of the speed along global x and y directions are not zero and this mean offset is constant over time. This is the effect of the drift velocity experienced by the vessel in the waves. The effect of this drift velocity is more prominent in the plot of the positions of the vessel shown in Figure 6c, where the linear trend in the global positions is visible.

In order to understand the variation of the drift velocity with frequency, the FFT of the velocity is computed and shown in Figure 6d. The x-velocity and y-velocity Fourier amplitudes show a large peak at the period corresponding to the period of the turning circle. However, it is also seen that the drift velocity is non-zero and manifests as a peak at the zero frequency. The total velocity Fourier amplitude shows a strong peak at the zero frequency and a smaller peak at the period of the turning circle. The presence of the drift velocity at the zero freqeuncy means that the drift velocity is constant across the turn and is not affected by the change in relative direction of the hull to the waves. This means that the drift velocity is a steady phenomenon that is independent of the relative direction of the hull to the waves.

From Figure 6a it can be seen that the dip in total velocity follows up right after the sway velocity attains its largest magnitude. This large sway velocity occurs due to the alignment of the drift velocity and the sway velocity experienced by the vessel in a calm water turn. The large sway velocity will lead to a large drag force on the vessel which eventually reduces its total speed. Due to the aspect ratio the hull can be thought of as an aerofoil section subjected to a large angle of attack that results in a considerable drag force. However, as the vessel turns into the waves, this drag reduces and eventually the ship tends to pick up speed. We believe the drop in total speed is attributed to the experience of this larger drag force when the drift velocity aligns with the sway direction of the vessel. Note that when at the diametrically opposite end of the circle, drift velocity opposes the sway velocity induced by the ship turning and thus this drag force is not large enough to cause a decrease in total speed.

The filtered yaw rate (to remove the effect of the first order yaw response of the vessel to waves) of the vessel over the steady drift path is shown in Figure 6e. It can be seen that the filtered yaw rate is fairly constant.

3.2. Drift Parameters

The experiments described in the previous section capture the influence of the following different values of four parameters on the drift:

- Wavelength of $0.8L$, $1.0L$ and $1.2L$

- Wave slope (H/λ) of 1/80, 1/60 and 1/40
- Rudder angle of 35° and −35°
- Propeller speed of 600 RPM, 700 RPM and 800 RPM that correspond to calm water Froude numbers 0.0508, 0.0602 and 0.0737 respectively for starboard turns and calm water Froude numbers 0.0538, 0.0627 and 0.0730 respectively for port turns

Note that the Froude number here is defined with respect to the total speed in the turn U_t and is shown in (1).

$$Fn = \frac{U_t}{\sqrt{gL}} \tag{1}$$

The focus of this study is to understand the drift parameters of the vessel in waves in a steady condition. Thus the first three turns (two turns in calm water and one turn in transient waves) are discarded from the analysis. The remaining data in steady waves is used to compute the drift parameters.

In the presence of waves, the vessel experiences a steady continuous drift and does not settle into a steady circle. Considering the origin to be located at the 0° course angle crossing (upcrossing for starboard turn and down crossing for port turn), the mathematical expression for the trajectory can be assumed to be of the form as shown in (2) and (3). Note that it is assumed that the vessel is at the origin at time $t = 0$.

$$\tilde{x}(t) = R\sin(\omega_{TC}t) + U_x t \tag{2}$$

$$\tilde{y}(t) = (-1)^m R(1 - \cos(\omega_{TC}t)) + U_y t \tag{3}$$

where R is the radius of the turn, ω_{TC} is the angular frequency of the turn and U_x and U_y denote the drift velocities of the circle in x and y directions respectively. For starboard turn $m = 0$ and for port turn $m = 1$. The time to complete one turn T_C is related to the angular frequency of the turn ω_{TC} as shown in (4).

$$\omega_{TC} = \frac{2\pi}{T_C} \tag{4}$$

The time to complete one turn T_C is obtained by calculating the time taken between two consecutive 0° (or 120° or 240°) course angle crossings. The other drift parameters R, U_x and U_y are obtained by fitting the mathematical expressions in (2) and (3) to the true data $x(t)$ and $y(t)$. The mean square error between the true trajectory and the mathematical expressions in (2) and (3) can be expressed as shown in (5).

$$E = \sum_{i=1}^{N} (\tilde{x}(t_i) - x(t_i))^2 + (\tilde{y}(t_i) - y(t_i))^2 \tag{5}$$

The drift parameters can be found by minimizing the error E. Analytically, the partial derivatives of E with respect to the drift parameters are set to zero and the resulting simultaneous equations are solved numerically using a Gauss-Seidel method where the latest estimates of the drift parameters are used to compute the next estimates. The Gauss-Seidel method is stopped when the change in the drift parameters is less than 10^{-6}.

$$\begin{aligned}\frac{\partial E}{\partial R} = 2\sum_{i=1}^{N} \big[&(R\sin(\omega_{TC}t_i) + U_x t_i - x(t_i))\sin(\omega_{TC}t_i) \\ &+((-1)^m R(1-\cos(\omega_{TC}t_i)) + U_y t_i - y(t_i))(-1)^m(1-\cos(\omega_{TC}t_i))\big] = 0\end{aligned} \tag{6}$$

$$\frac{\partial E}{\partial U_x} = 2\sum_{i=1}^{N} [(R\sin(\omega_{TC}t_i) + U_x t_i - x(t_i))t_i] = 0 \tag{7}$$

$$\frac{\partial E}{\partial U_y} = 2\sum_{i=1}^{N}\left[((-1)^m R(1-\cos(\omega_{TC}t_i)) + U_y t_i - y(t_i))t_i\right] = 0 \tag{8}$$

The best and the worst fits are shown in Figure 7. The best fit is the one that is closest to the true path and is found to be for the case of port turn at propeller speed of 800 RPM, $H/\lambda = 1/40$ and $\lambda/L = 1.00$ between 240° course angle crossings of second steady turn. The worst fit is the one that is farthest from the true path within the collected data and is found to be for the case of starboard turn at propeller speed of 600 RPM, $H/\lambda = 1/40$ and $\lambda/L = 0.80$ between 0° course angle crossings of first steady turn. The root mean square error (RMSE) of the best fit is 2.40 m and the RMSE of the worst fit is 7.59 m.

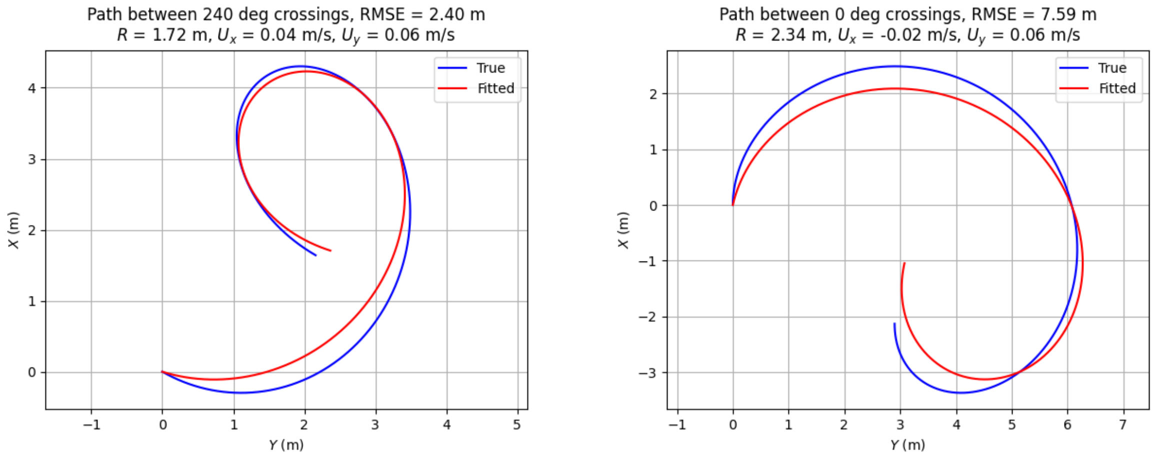

(a) Best fit

(b) Worst fit

Figure 7: Best and worst path fits within the dataset

The normalized histogram of the RMSE of the fits is shown in Figure 8. The corresponding fit of a log-normal distribution is also shown. It can be seen that the distribution fits the tails of the data well but not the center. The data demonstrates a bimodal distribution but the fitted log-normal distribution is unimodal.

In addition to parameters obtained from the fit, the drift distance Δ_d and drift direction θ_d are computed. The drift distance Δ_d is computed as the Eucledian distance between consecutive locations of the ship in a turn when its course is oriented in a specific direction. The drift direction θ_d is computed as the direction of the drift. The relative drift direction is defined as shown in (9)

$$\gamma_d = \text{sign}(\delta)(\theta_d - \beta_w) = \text{sign}(\delta)\left(\tan^{-1}\left(\frac{\Delta_y}{\Delta_x}\right) - \beta_w\right) \tag{9}$$

where δ is the rudder angle, β_w is the direction of propagation of the incident waves and Δ_x and Δ_y are the drift distances in the x and y directions respectively. The relative drift direction is measured in degrees.

Thus the drift parameters computed for each turning circle are:

- Radius of turn R
- Time to complete one turn T_C
- Total drift velocity $U_d = \sqrt{U_x^2 + U_y^2}$
- Relative drift direction γ_d
- Drift distance Δ_d between consecutive 0° (or 120° or 240°) course angle crossings

The drift parameters are non-dimensionalized as shown below:

- Radius of turn $R' = R/L$

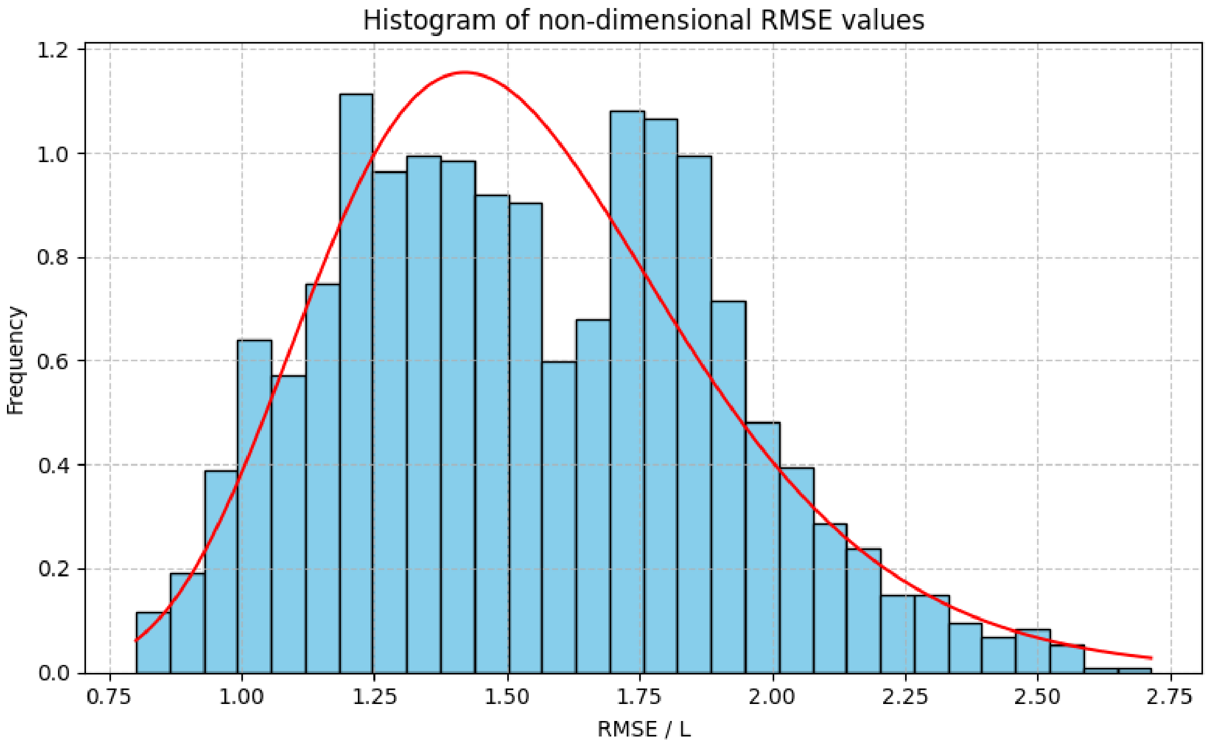

(a) RMSE of the fits

Figure 8: Normalized histogram of the RMSE of the fits. The red line shows the fit of a log-normal distribution with shape parameter $\sigma = 0.2366$ and scale parameter $s = \exp(\mu) = 1.5026$.

- Time to complete one turn $T'_C = T_C U_{des}/L$
- Total drift velocity $U'_d = U_d/U_{des}$
- Relative drift direction γ_d (dimensionless)
- Drift distance $\Delta'_d = \Delta_d/L$

Note that the velocity used for non-dimensionalization of the drift parameters is the fixed design speed of the vessel $U_{des} = 0.759$ m/s (corresponding to $Fn_{des} = 0.142$) rather than the speed of the vessel during the calm water turn U_t. This is chosen so in this study to keep the effect of independent variables (particularly propeller speed) from influencing the non-dimensionalized drift parameters.

All the drift parameters computed for different parameter sweep are reported in Appendix A.

3.2.1. Drift parameter variation with rudder angle

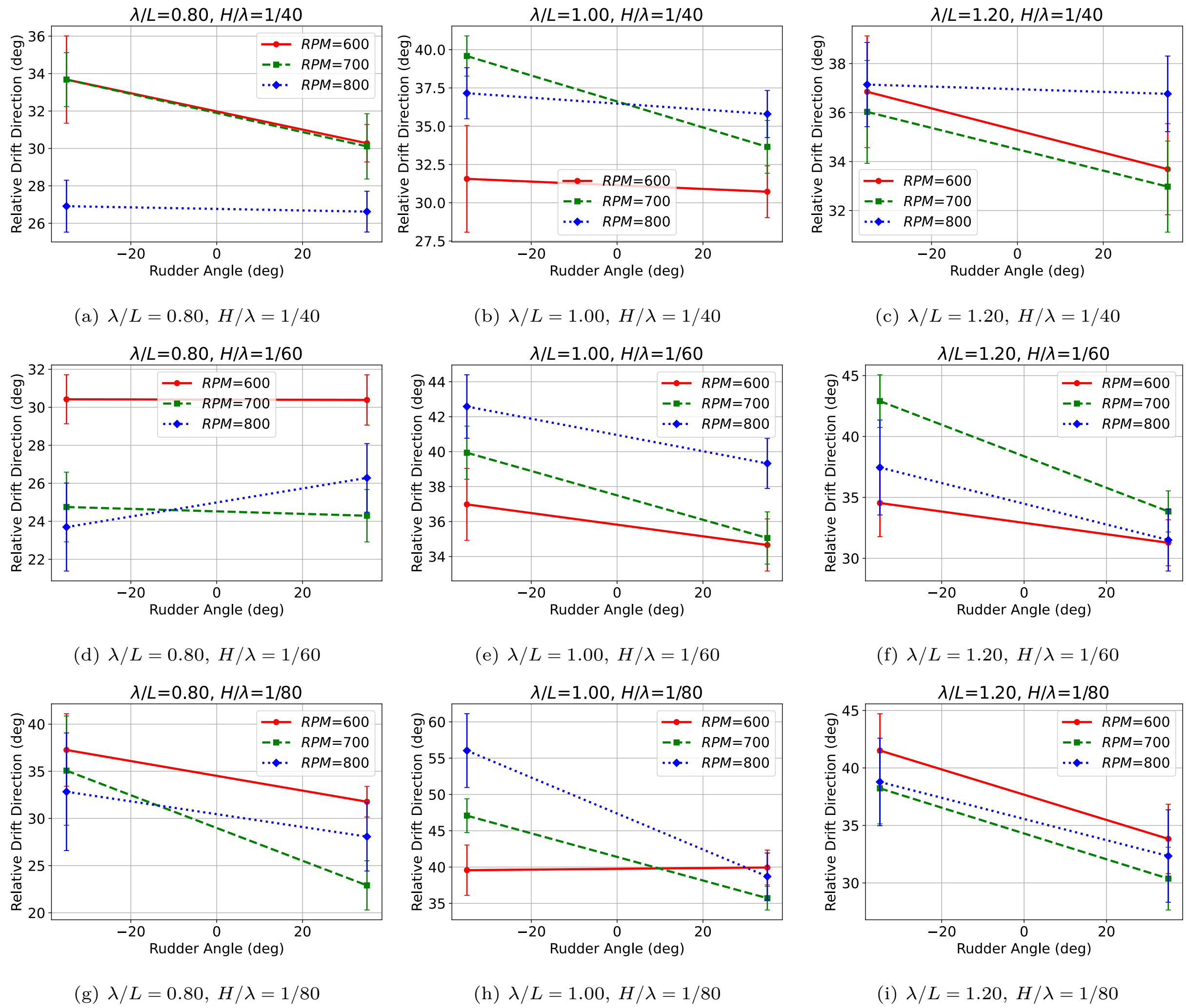

(a) $\lambda/L = 0.80,\ H/\lambda = 1/40$ (b) $\lambda/L = 1.00,\ H/\lambda = 1/40$ (c) $\lambda/L = 1.20,\ H/\lambda = 1/40$

(d) $\lambda/L = 0.80,\ H/\lambda = 1/60$ (e) $\lambda/L = 1.00,\ H/\lambda = 1/60$ (f) $\lambda/L = 1.20,\ H/\lambda = 1/60$

(g) $\lambda/L = 0.80,\ H/\lambda = 1/80$ (h) $\lambda/L = 1.00,\ H/\lambda = 1/80$ (i) $\lambda/L = 1.20,\ H/\lambda = 1/80$

Figure 9: Variation of drift direction (obtained from the fit) with rudder angle (The vertical bars at each data point represent the 95% confidence interval of the reported mean value). Solid line indicates 600 RPM, dashed line indicates 700 RPM and dotted line indicates 800 RPM at model scale.

Figure 9 shows the variation of relative drift direction with rudder angle for different wavelengths, wave slopes and propeller speeds. It can be seen that the relative drift direction is marginally less for starboard turns as compared to the port turns for all combinations of propeller speed, wave slope and wavelength.

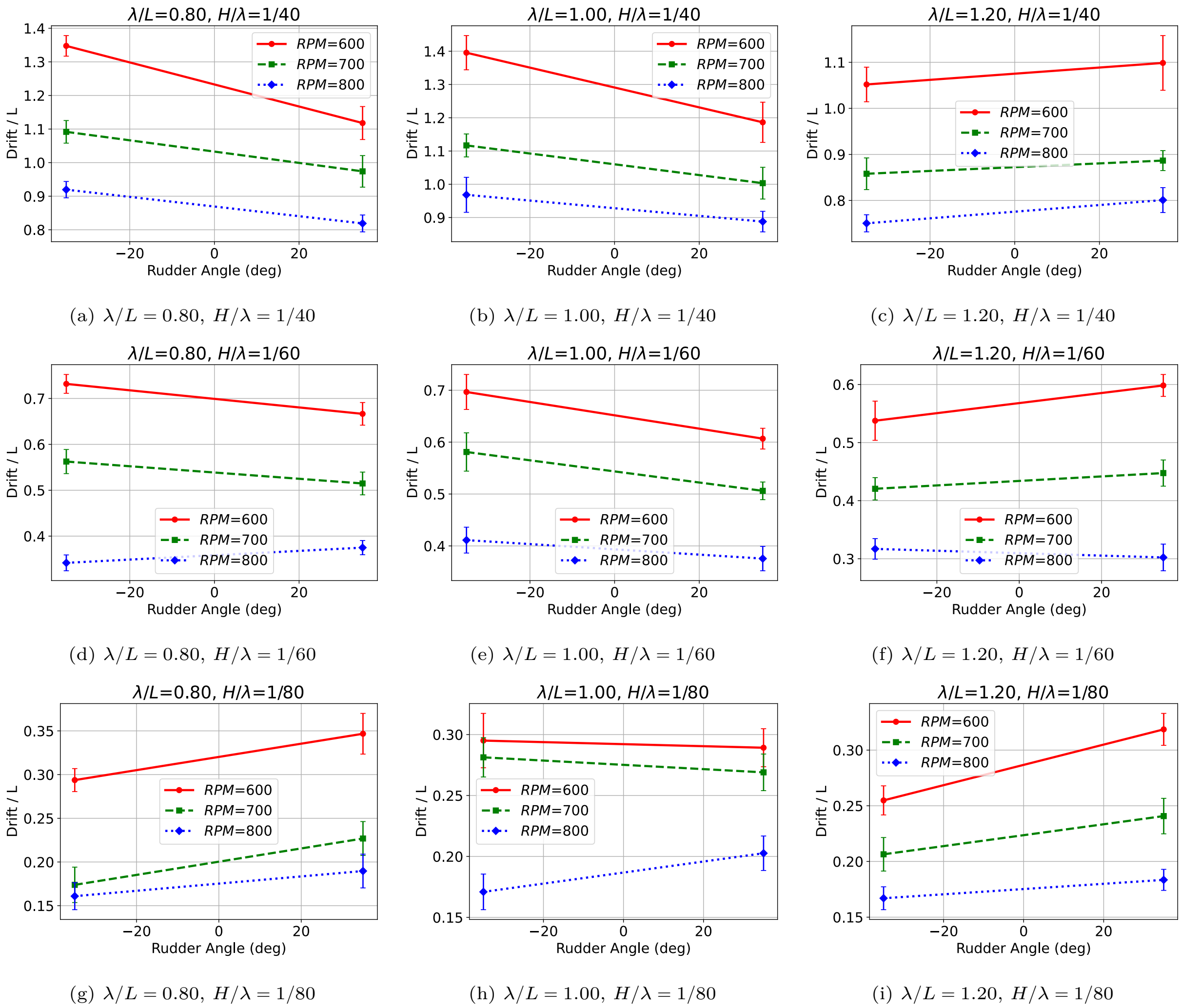

(a) $\lambda/L = 0.80,\ H/\lambda = 1/40$ (b) $\lambda/L = 1.00,\ H/\lambda = 1/40$ (c) $\lambda/L = 1.20,\ H/\lambda = 1/40$

(d) $\lambda/L = 0.80,\ H/\lambda = 1/60$ (e) $\lambda/L = 1.00,\ H/\lambda = 1/60$ (f) $\lambda/L = 1.20,\ H/\lambda = 1/60$

(g) $\lambda/L = 0.80,\ H/\lambda = 1/80$ (h) $\lambda/L = 1.00,\ H/\lambda = 1/80$ (i) $\lambda/L = 1.20,\ H/\lambda = 1/80$

Figure 10: Variation of drift distance with rudder angle (The vertical bars at each data point represent the 95% confidence interval of the reported mean value). Solid line indicates 600 RPM, dashed line indicates 700 RPM and dotted line indicates 800 RPM at model scale.

Figure 10 shows the variation of drift distance with rudder angle for different combinations of wavelengths, wave slopes and propeller speeds. At $\lambda/L = 1.00$, the starboard turns have a marginally lower drift distance than the port turns at most propeller speeds. The exception to this is the case of $\lambda/L = 1.00$, $H/\lambda = 1/80$ and 800 RPM where the port turns have a lower drift distance than the starboard turns. However, the variation in drift distances is quite small. This trend is also not preserved for $\lambda/L = 0.80$ and 1.20. Thus, the data suggests that the drift distance is independent of the rudder angle.

Conventional maneuvering models for single-screw vessels (such as the MMG model described by Yasukawa and Yoshimura [21]) typically incorporate rudder-propeller interactions to account for asymmetric turning characteristics between port and starboard maneuvers. However, the experimental results of this study reveal no significant difference in drift distances or relative drift directions between port and starboard turns across various propeller speeds. This finding suggests that rudder-propeller interactions have minimal influence on drift behavior. This observation aligns with the physical understanding that the drift forces originate from hull-wave interactions rather than propulsion and steering effects.

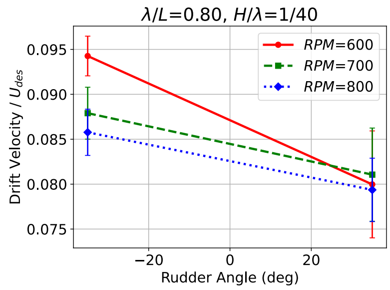

(a) $\lambda/L = 0.80,\ H/\lambda = 1/40$

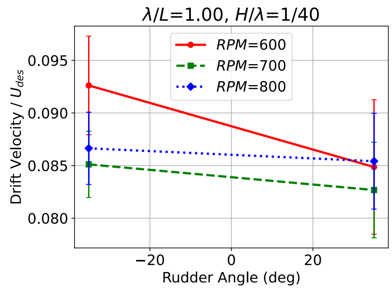

(b) $\lambda/L = 1.00,\ H/\lambda = 1/40$

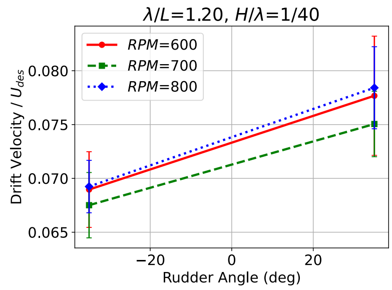

(c) $\lambda/L = 1.20,\ H/\lambda = 1/40$

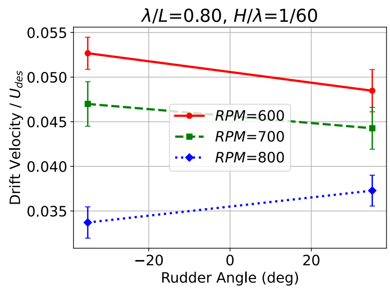

(d) $\lambda/L = 0.80,\ H/\lambda = 1/60$

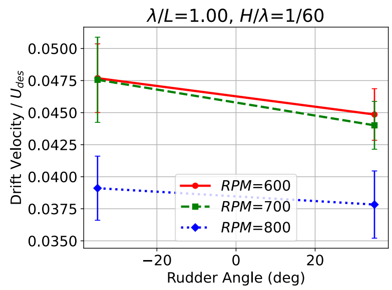

(e) $\lambda/L = 1.00,\ H/\lambda = 1/60$

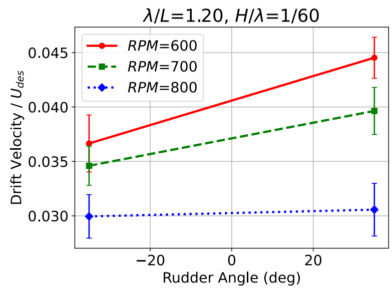

(f) $\lambda/L = 1.20,\ H/\lambda = 1/60$

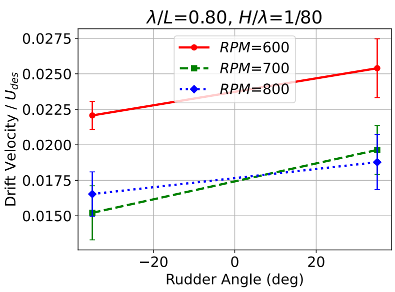

(g) $\lambda/L = 0.80,\ H/\lambda = 1/80$

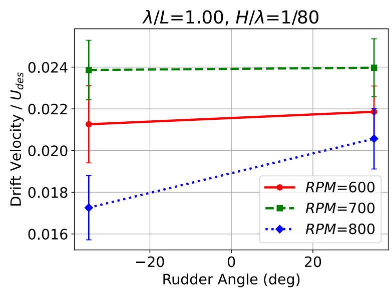

(h) $\lambda/L = 1.00,\ H/\lambda = 1/80$

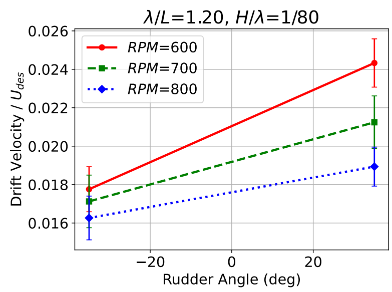

(i) $\lambda/L = 1.20,\ H/\lambda = 1/80$

Figure 11: Variation of drift velocity (obtained from the fit) with rudder angle (The vertical bars at each data point represent the 95% confidence interval of the reported mean value). Solid line indicates 600 RPM, dashed line indicates 700 RPM and dotted line indicates 800 RPM at model scale.

Figure 11 shows the variation of drift velocity with rudder angle. While a clear trend does not exist at

$\lambda/L = 0.80$ and $\lambda/L = 1.00$, at $\lambda/L = 1.20$ the drift velocity is marginally higher for the starboard turns as compared to the port turns.

It can be seen that the variation in drift velocity with rudder angle is not significantly larger than the confidence interval. This suggests that the drift velocity does not significantly differ between the port and starboard turns. This observation aligns with the physical understanding that the drift forces originate due to hull-wave interaction and are not significantly affected by steering and propulsion parameters.

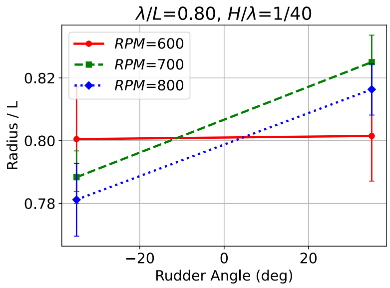

(a) $\lambda/L = 0.80,\ H/\lambda = 1/40$

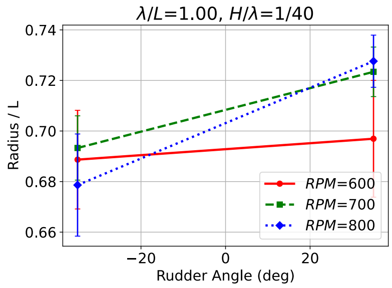

(b) $\lambda/L = 1.00,\ H/\lambda = 1/40$

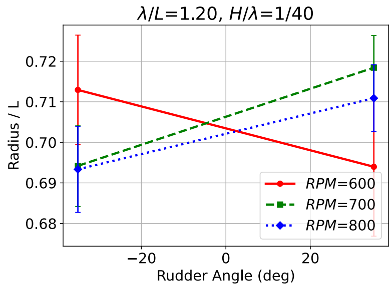

(c) $\lambda/L = 1.20,\ H/\lambda = 1/40$

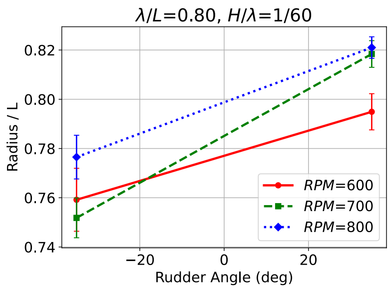

(d) $\lambda/L = 0.80,\ H/\lambda = 1/60$

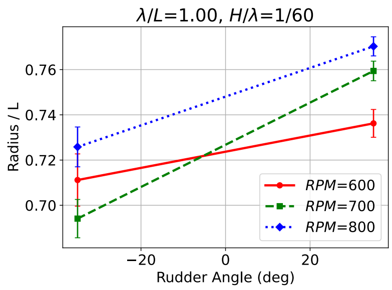

(e) $\lambda/L = 1.00,\ H/\lambda = 1/60$

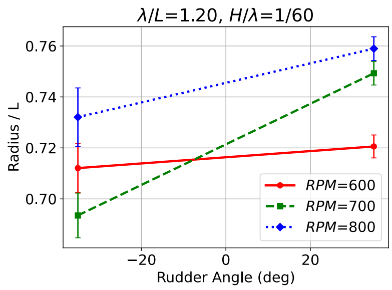

(f) $\lambda/L = 1.20,\ H/\lambda = 1/60$

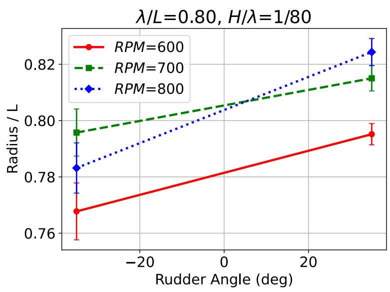

(g) $\lambda/L = 0.80,\ H/\lambda = 1/80$

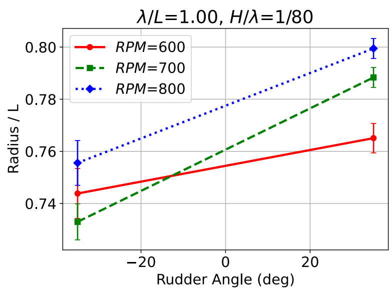

(h) $\lambda/L = 1.00,\ H/\lambda = 1/80$

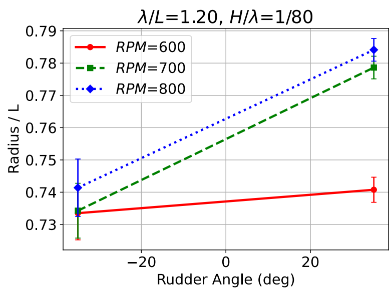

(i) $\lambda/L = 1.20,\ H/\lambda = 1/80$

Figure 12: Variation of radius of turn (obtained from the fit) with rudder angle (The vertical bars at each data point represent the 95% confidence interval of the reported mean value). Solid line indicates 600 RPM, dashed line indicates 700 RPM and dotted line indicates 800 RPM at model scale.

Figure 12 shows the variation of the radius of the turn with the rudder angle for different combinations of propeller speeds, wave slopes and wavelengths. It can be seen that the radius of the turn is marginally more for the starboard turns as compared to the port turns. The only exception to this trend is at $\lambda/L = 1.00$ and $\lambda/L = 1.20$ for $H/\lambda = 1/40$ and 600 RPM where the port turns have a higher radius of turn as compared to the starboard turns. The marginal variation between the port and starboard turn radii can be attributed to the asymmetry due to the presence of a single screw propeller [21, 22].

Figure 13 shows the variation of turning circle times with rudder angles for different combinations of

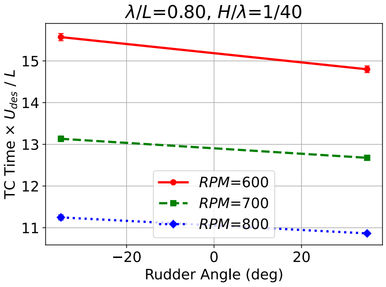

(a) $\lambda/L = 0.80,\ H/\lambda = 1/40$

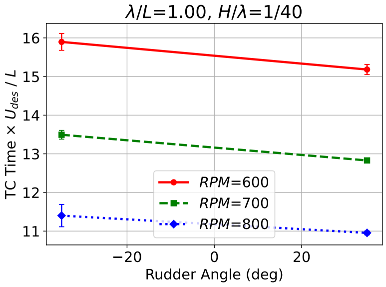

(b) $\lambda/L = 1.00,\ H/\lambda = 1/40$

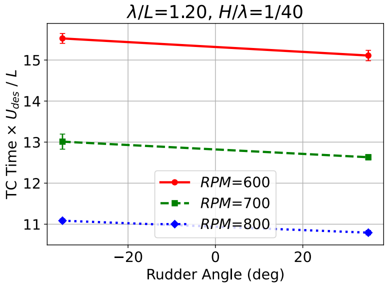

(c) $\lambda/L = 1.20,\ H/\lambda = 1/40$

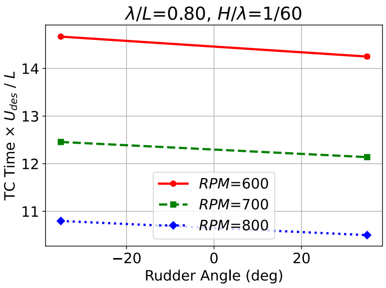

(d) $\lambda/L = 0.80,\ H/\lambda = 1/60$

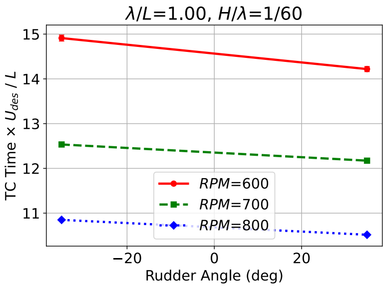

(e) $\lambda/L = 1.00,\ H/\lambda = 1/60$

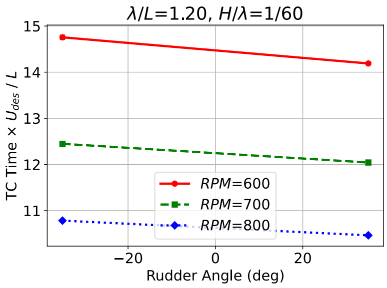

(f) $\lambda/L = 1.20,\ H/\lambda = 1/60$

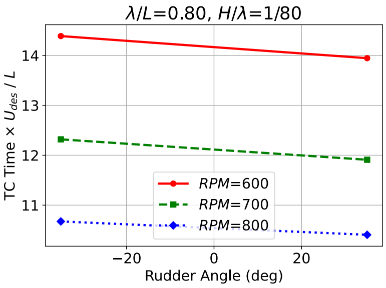

(g) $\lambda/L = 0.80,\ H/\lambda = 1/80$

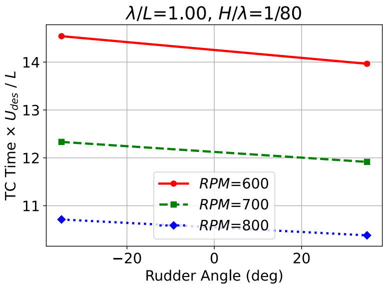

(h) $\lambda/L = 1.00,\ H/\lambda = 1/80$

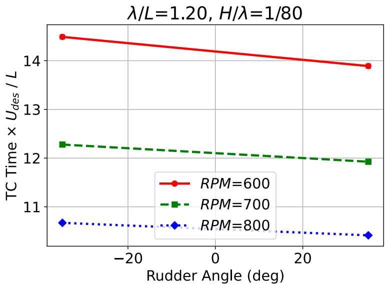

(i) $\lambda/L = 1.20,\ H/\lambda = 1/80$

Figure 13: Variation of time to complete one turn (obtained from the fit) with rudder angle (The vertical bars at each data point represent the 95% confidence interval of the reported mean value). Solid line indicates 600 RPM, dashed line indicates 700 RPM and dotted line indicates 800 RPM at model scale.

propeller speeds, wavelengths and wave slopes. It can be seen that the turning circle times for starboard turns are less than the corresponding port turns. This trend is uniformly observed for all combinations of wave slopes, wavelengths and propeller speeds. The confidence interval of the turning circle times is much smaller than the observed variation in times between port and starboard turns indicating a statistically significant variation.

3.2.2. Drift parameter variation with propeller speed

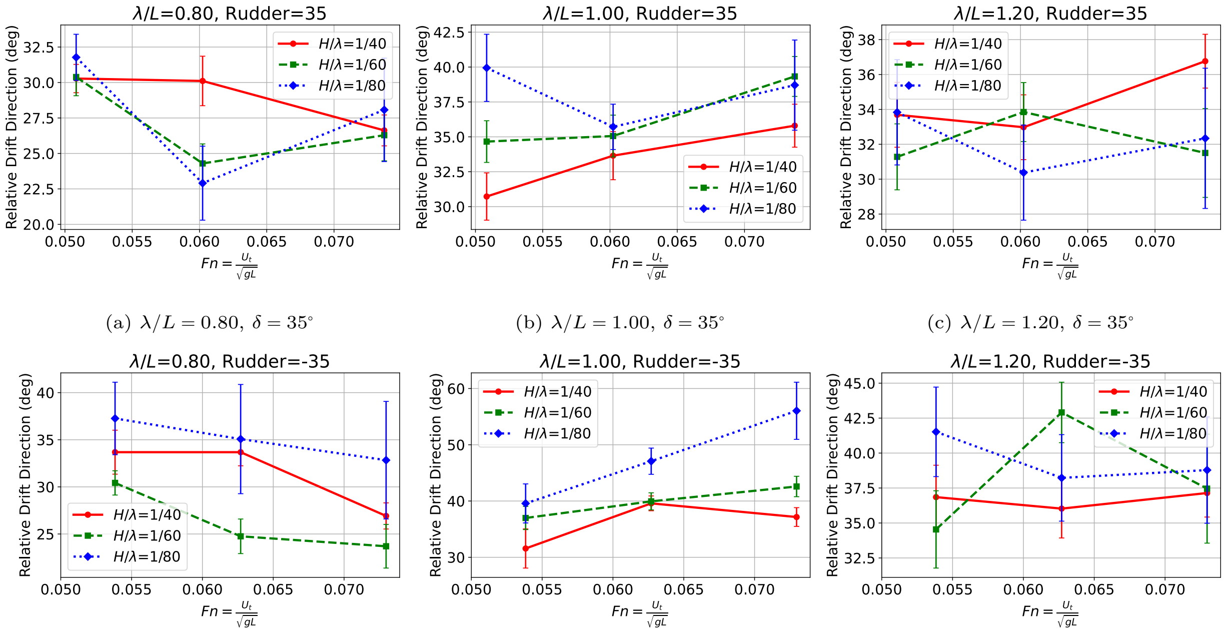

(a) $\lambda/L = 0.80,\ \delta = 35^{\circ}$ (b) $\lambda/L = 1.00,\ \delta = 35^{\circ}$ (c) $\lambda/L = 1.20,\ \delta = 35^{\circ}$

(d) $\lambda/L = 0.80,\ \delta = -35^{\circ}$ (e) $\lambda/L = 1.00,\ \delta = -35^{\circ}$ (f) $\lambda/L = 1.20,\ \delta = -35^{\circ}$

Figure 14: Variation of drift direction (obtained from the fit) with propeller speed (The vertical bars at each data point represent the 95% confidence interval of the reported mean value). Solid line indicates $H/\lambda = 1/40$, dashed line indicates $H/\lambda = 1/60$ and dotted line indicates $H/\lambda = 1/80$

Figure 14 shows the variation of relative drift direction with propeller speed for different combinations of wavelengths, wave slopes and rudder angles. It can be seen that the relative drift direction does not show a statistically significant variation with propeller speed for all combinations of λ/L, H/λ and rudder angles. Thus, the data suggests that the relative drift direction is independent of the propeller speed. Since the propeller speed primarily influences the forward speed of the ship, this observation suggests that the net direction of the drift is independent of the forward speed of the ship.

Figure 15 shows the variation of drift distance with propeller speed for different combinations of wavelengths, wave slopes and rudder angles. It can be seen that the drift distance is higher for lower propeller speeds and this trend is observed for all wavelengths, wave slopes and rudder angles. Thus, the data suggests that the drift distance decreases with the propeller speed. It will be seen later that this can be attributed to a decrease in the time to complete one turn as shown in Figure 18.

Figure 16 shows the variation of drift velocity with the forward speed of the vessel for different combinations of wave slopes, wavelengths and rudder angles. It can be seen that the drift velocity is fairly constant with Froude number in turn. This statistically significant trend is uniformly observed across different wave slopes, wavelengths and rudder angles. This indicates that although the drift distance is decreasing with forward speed (as seen in Figure 15) the drift velocity remains fairly constant across different forward speeds.

Figure 17 shows the variation of radius of turn with propeller speed for different combinations of wave-

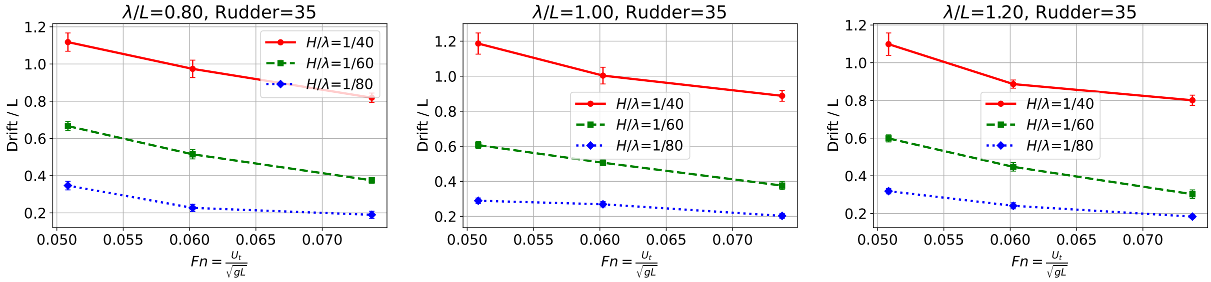

(a) $\lambda/L = 0.80,\ \delta = 35^{\circ}$

(b) $\lambda/L = 1.00,\ \delta = 35^{\circ}$

(c) $\lambda/L = 1.20,\ \delta = 35^{\circ}$

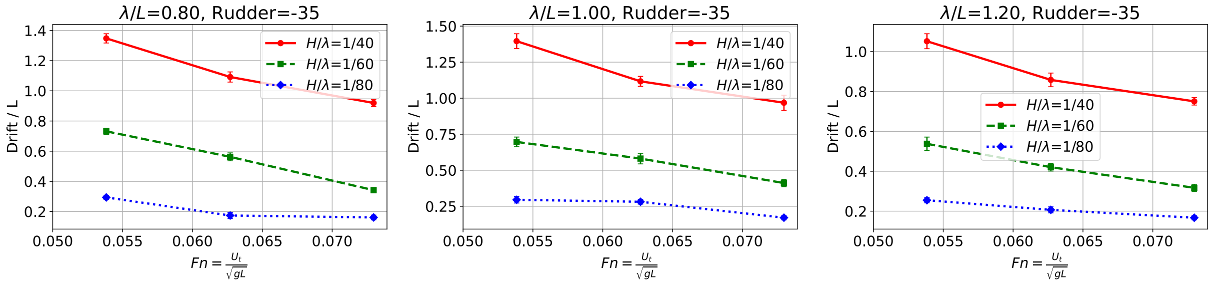

(d) $\lambda/L = 0.80,\ \delta = -35^{\circ}$

(e) $\lambda/L = 1.00,\ \delta = -35^{\circ}$

(f) $\lambda/L = 1.20,\ \delta = -35^{\circ}$

Figure 15: Variation of drift distance with propeller speed (The vertical bars at each data point represent the 95% confidence interval of the reported mean value). Solid line indicates $H/\lambda = 1/40$, dashed line indicates $H/\lambda = 1/60$ and dotted line indicates $H/\lambda = 1/80$

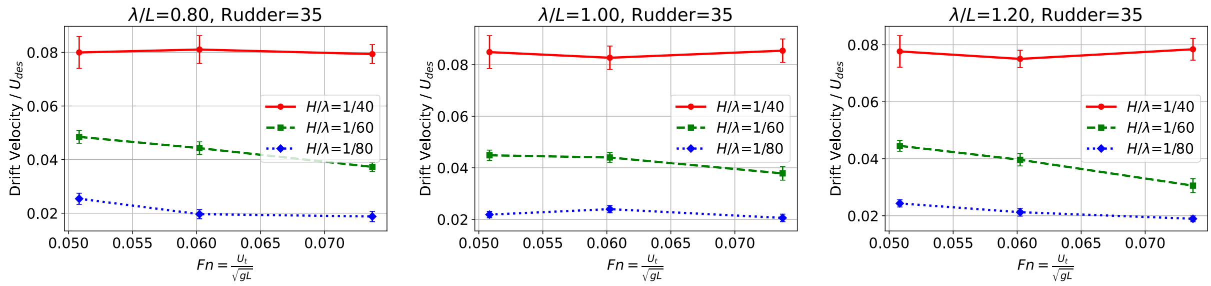

(a) $\lambda/L = 0.80,\ \delta = 35^{\circ}$

(b) $\lambda/L = 1.00,\ \delta = 35^{\circ}$

(c) $\lambda/L = 1.20,\ \delta = 35^{\circ}$

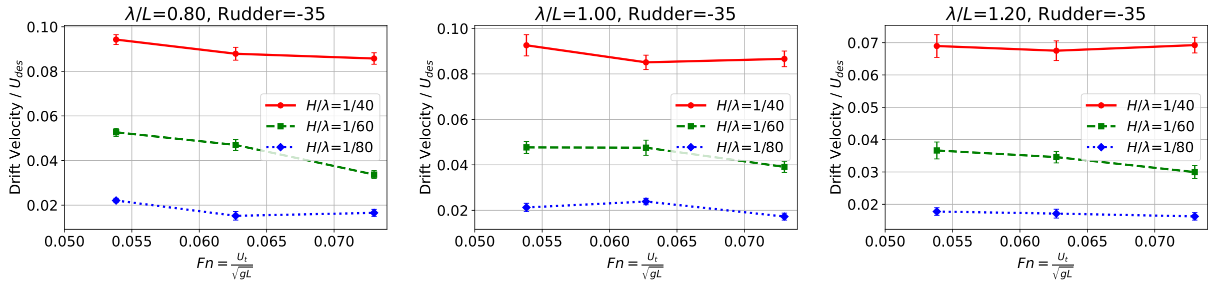

(d) $\lambda/L = 0.80,\ \delta = -35^{\circ}$

(e) $\lambda/L = 1.00,\ \delta = -35^{\circ}$

(f) $\lambda/L = 1.20,\ \delta = -35^{\circ}$

Figure 16: Variation of drift velocity (obtained from the fit) with forward speed (The vertical bars at each data point represent the 95% confidence interval of the reported mean value). Solid line indicates $H/\lambda = 1/40$, dashed line indicates $H/\lambda = 1/60$ and dotted line indicates $H/\lambda = 1/80$

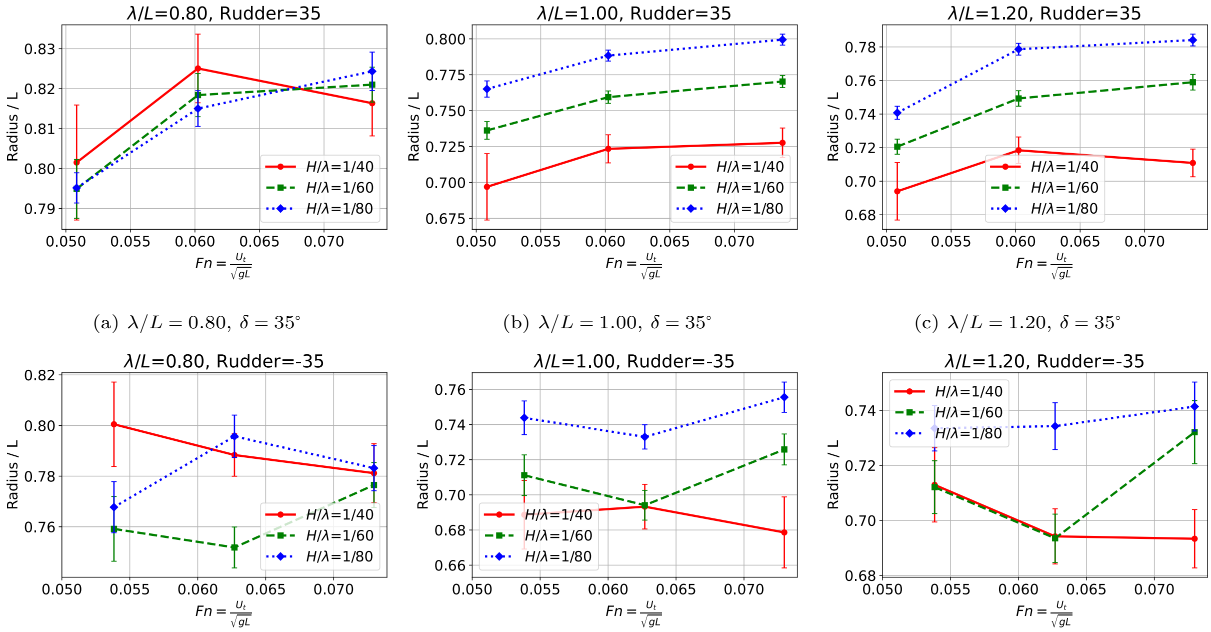

(a) $\lambda/L = 0.80,\ \delta = 35^\circ$ (b) $\lambda/L = 1.00,\ \delta = 35^\circ$ (c) $\lambda/L = 1.20,\ \delta = 35^\circ$

(d) $\lambda/L = 0.80,\ \delta = -35^\circ$ (e) $\lambda/L = 1.00,\ \delta = -35^\circ$ (f) $\lambda/L = 1.20,\ \delta = -35^\circ$

Figure 17: Variation of radius of turn (obtained from the fit) with propeller speed (The vertical bars at each data point represent the 95% confidence interval of the reported mean value). Solid line indicates $H/\lambda = 1/40$, dashed line indicates $H/\lambda = 1/60$ and dotted line indicates $H/\lambda = 1/80$

lengths, wave slopes and rudder angles. It can be seen that the radii of starboard turns increase with propeller speeds for all wave slopes and rudder angles at $\lambda/L = 1.00$ and 1.20. At $\lambda/L = 0.80$, the radius of starboard turn is almost constant with propeller speed. For the port turns, the radius of turn is almost constant with propeller speed across all wave slopes and wavelengths. Thus, the data suggests that the radius of the turn is independent of the forward speed of the ship.

Figure 18 shows the variation of time to complete one turn with propeller speed for different combinations of wavelengths, wave slopes and rudder angles. It can be seen that the time to complete one turn reduces with an increase in forward speed. This trend is observed for all combinations of wavelengths, wave slopes and rudder angles. This is consistent with the results shown in Figure 17 that as the forward speed increases, the radius of the turn remains fairly constant and hence the time to complete one turn decreases.

From Figure 15 and Figure 16, it is seen that the drift distance decreases with forward speed but the drift velocity remains constant. Figure 18 shows that as the forward speed increases, the time to complete one turn decreases. This indicates that the observed decrease in drift distance with forward speed occurs primarily due to the decrease in time to complete one turn.

3.2.3. Drift parameter variation with wave slope

Figure 19 shows the variation of relative drift direction with wave slope for different combinations of wavelengths, propeller speeds and rudder angles. It can be seen that the relative drift direction does not show a statistically significant variation with wave slope for all combinations of λ/L, H/λ and rudder angles. The relative drift direction is independent of the wave slope. This observation is consistent with the physical understanding that the drift force is primarily due to the interaction between the hull and waves and the higher wave height just increases the magnitude of the drift force and does not affect the direction of the force.

Figure 20 shows the variation of drift distance with wave slope for different combinations of wavelengths,

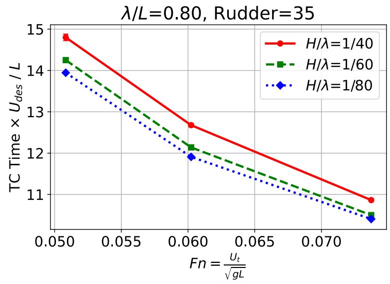

(a) $\lambda/L = 0.80,\ \delta = 35^{\circ}$

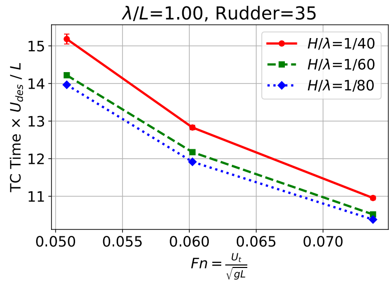

(b) $\lambda/L = 1.00,\ \delta = 35^{\circ}$

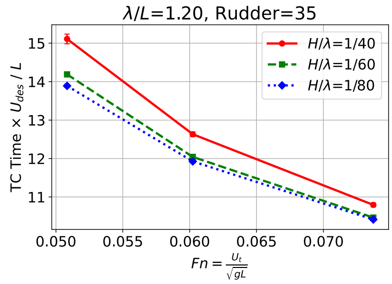

(c) $\lambda/L = 1.20,\ \delta = 35^{\circ}$

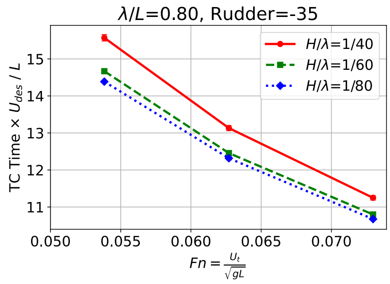

(d) $\lambda/L = 0.80,\ \delta = -35^{\circ}$

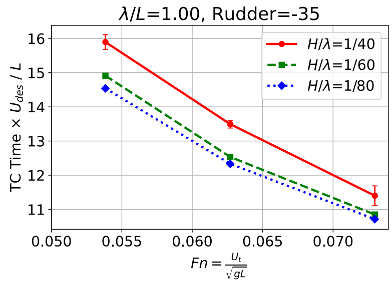

(e) $\lambda/L = 1.00,\ \delta = -35^{\circ}$

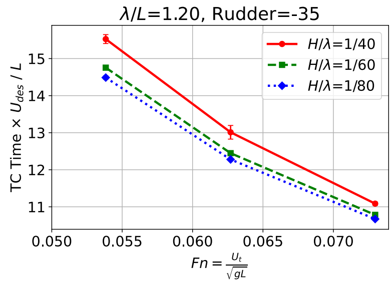

(f) $\lambda/L = 1.20,\ \delta = -35^{\circ}$

Figure 18: Variation of time to complete one turn (obtained from the fit) with propeller speed (The vertical bars at each data point represent the 95% confidence interval of the reported mean value). Solid line indicates $H/\lambda = 1/40$, dashed line indicates $H/\lambda = 1/60$ and dotted line indicates $H/\lambda = 1/80$

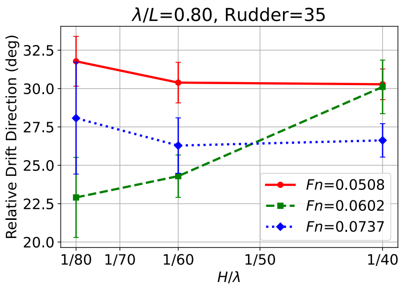

(a) $\lambda/L = 0.80,\ \delta = 35^{\circ}$

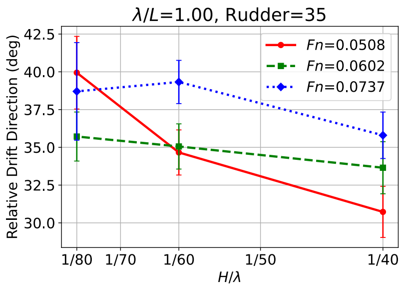

(b) $\lambda/L = 1.00,\ \delta = 35^{\circ}$

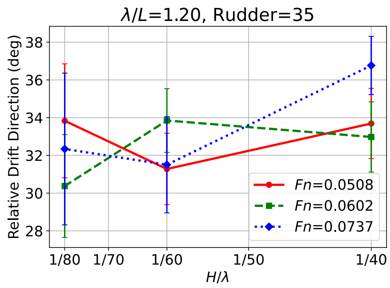

(c) $\lambda/L = 1.20,\ \delta = 35^{\circ}$

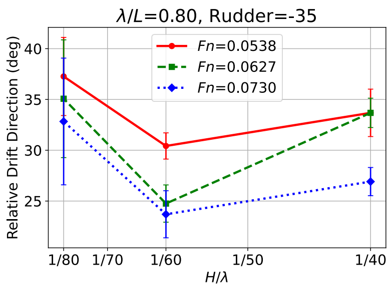

(d) $\lambda/L = 0.80,\ \delta = -35^{\circ}$

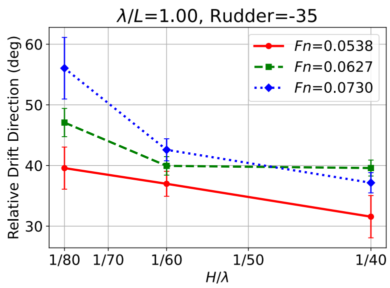

(e) $\lambda/L = 1.00,\ \delta = -35^{\circ}$

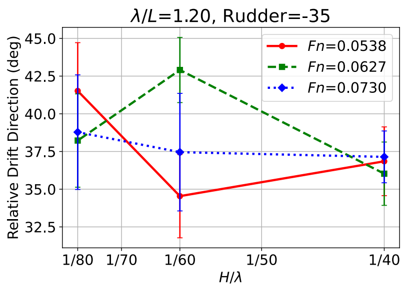

(f) $\lambda/L = 1.20,\ \delta = -35^{\circ}$

Figure 19: Variation of drift direction (obtained from the fit) with wave slope (The vertical bars at each data point represent the 95% confidence interval of the reported mean value). Solid line indicates 600 RPM, dashed line indicates 700 RPM and dotted line indicates 800 RPM

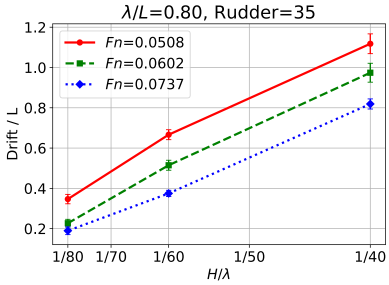

(a) $\lambda/L = 0.80,\ \delta = 35^{\circ}$

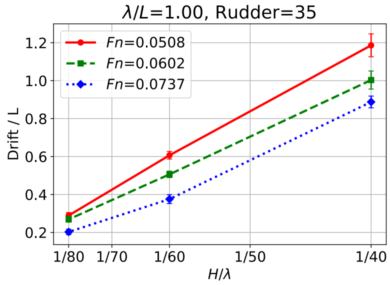

(b) $\lambda/L = 1.00,\ \delta = 35^{\circ}$

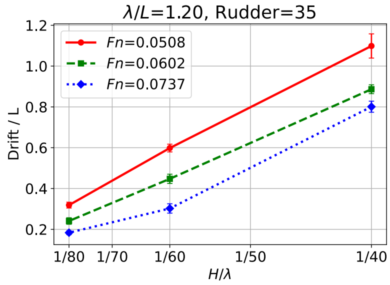

(c) $\lambda/L = 1.20,\ \delta = 35^{\circ}$

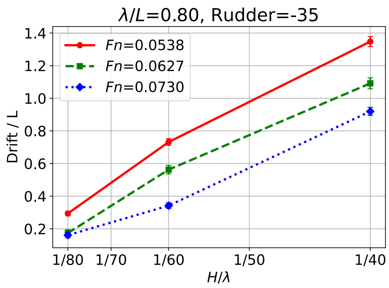

(d) $\lambda/L = 0.80,\ \delta = -35^{\circ}$

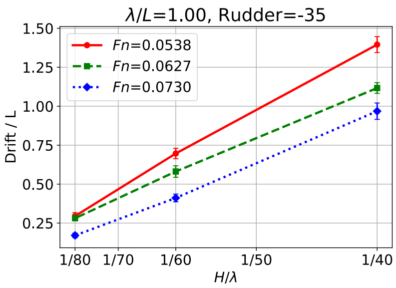

(e) $\lambda/L = 1.00,\ \delta = -35^{\circ}$

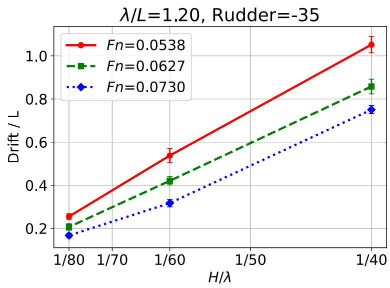

(f) $\lambda/L = 1.20,\ \delta = -35^{\circ}$

Figure 20: Variation of drift distance with wave slope (The vertical bars at each data point represent the 95% confidence interval of the reported mean value). Solid line indicates 600 RPM, dashed line indicates 700 RPM and dotted line indicates 800 RPM

propeller speeds and rudder angles. It can be seen that the drift distance is higher for higher wave slopes and this trend is observed for all combinations of wavelengths, propeller speeds and rudder angles. Thus the data suggests that the drift distance increases with the wave slope. This observation is in line with the results reported by [14].

Figure 21 shows the variation of drift velocity with wave slope for different combinations of wavelengths, propeller speeds and rudder angles. It can be seen that the drift velocity is higher for higher wave slopes. The data suggests that the drift velocity increases linearly with the wave slope. However, there is a need to conduct these experiments at more wave slopes to ascertain the slope of the line accurately. While the slope might not be estimated accurately, the linear trend is observed uniformly across five different repeated experiments across three wavelength to length ratios, three different propeller RPMs and for port and starboard turns alike. Therefore, it can be concluded that the drift velocity is purely a function of the hull geometry and its interaction with the wave. This is an interesting result that has not previously been reported in the literature to our knowledge.

It is well known that the drift forces in a monochromatic wave field are proportional to the square of the wave height. However, the drift velocity is observed to vary linearly with wave height. The exact physics that governs this linear relationship is not clear yet and needs further theoretical and experimental investigations.

Figure 22 shows the variation of radius of turn with wave slope for different combinations of wavelengths, propeller speeds and rudder angles. It can be seen that the radius of turn is fairly independent of the wave slope across all combinations of wavelengths, propeller speeds and rudder angles. Thus it seems the presence of the waves does not significantly affect the notionally calculated radius of turn.

Figure 23 shows the variation of time to complete one turn with wave slope for different combinations of wavelengths, propeller speeds and rudder angles. It can be seen that the time to complete one turn marginally increases with wave slope and this effect is observed for all combinations of wavelengths, propeller speeds

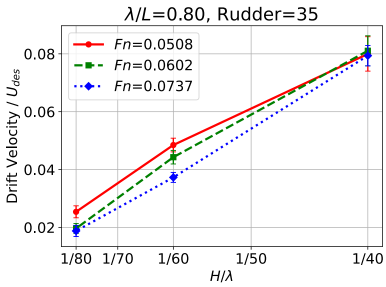

(a) $\lambda/L = 0.80,\ \delta = 35^{\circ}$

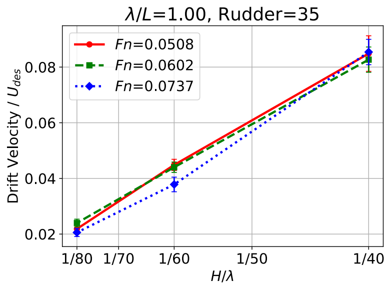

(b) $\lambda/L = 1.00,\ \delta = 35^{\circ}$

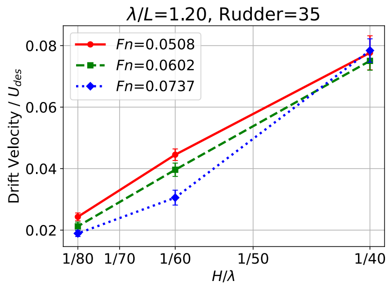

(c) $\lambda/L = 1.20,\ \delta = 35^{\circ}$

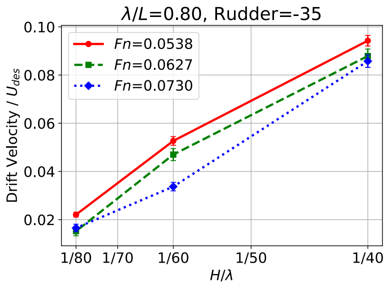

(d) $\lambda/L = 0.80,\ \delta = -35^{\circ}$

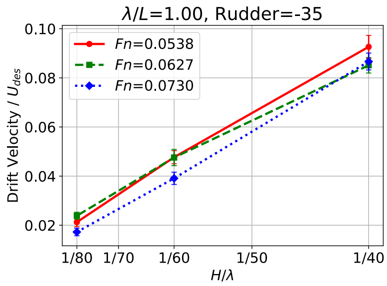

(e) $\lambda/L = 1.00,\ \delta = -35^{\circ}$

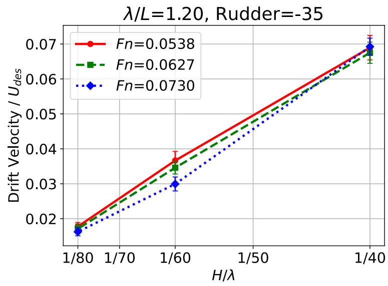

(f) $\lambda/L = 1.20,\ \delta = -35^{\circ}$

Figure 21: Variation of drift velocity (obtained from the fit) with wave slope (The vertical bars at each data point represent the 95% confidence interval of the reported mean value). Solid line indicates 600 RPM, dashed line indicates 700 RPM and dotted line indicates 800 RPM

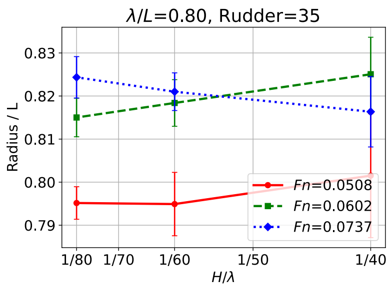

(a) $\lambda/L = 0.80,\ \delta = 35^{\circ}$

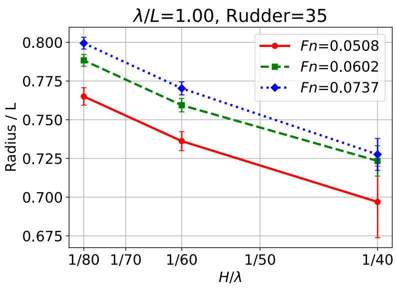

(b) $\lambda/L = 1.00,\ \delta = 35^{\circ}$

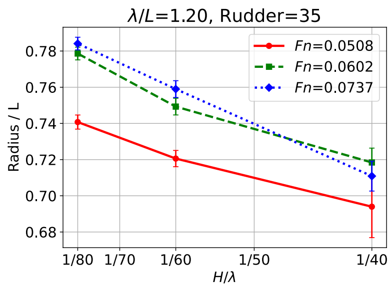

(c) $\lambda/L = 1.20,\ \delta = 35^{\circ}$

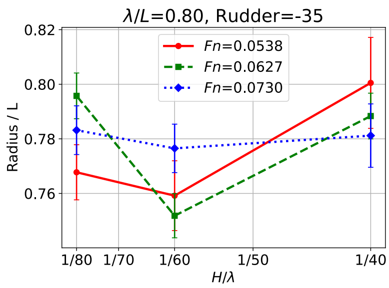

(d) $\lambda/L = 0.80,\ \delta = -35^{\circ}$

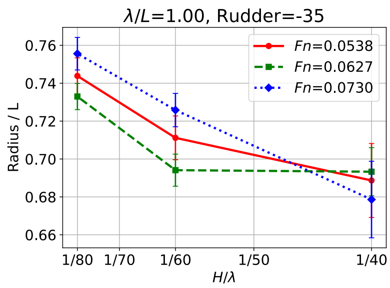

(e) $\lambda/L = 1.00,\ \delta = -35^{\circ}$

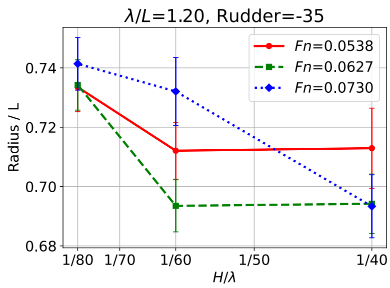

(f) $\lambda/L = 1.20,\ \delta = -35^{\circ}$

Figure 22: Variation of radius of turn (obtained from the fit) with wave slope (The vertical bars at each data point represent the 95% confidence interval of the reported mean value). Solid line indicates 600 RPM, dashed line indicates 700 RPM and dotted line indicates 800 RPM

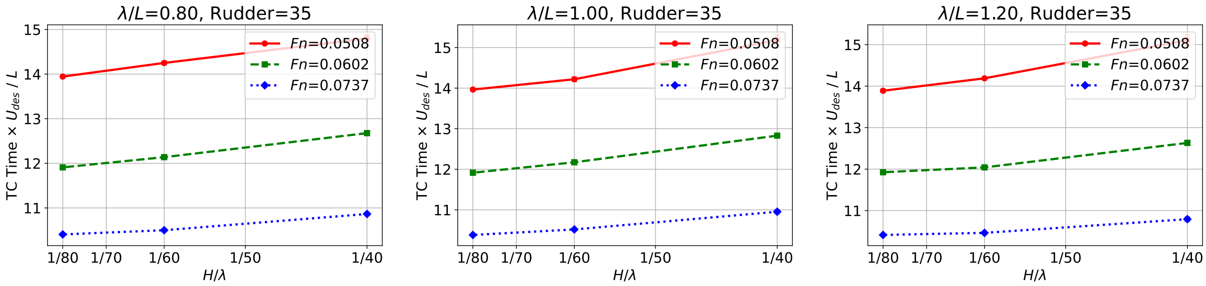

(a) $\lambda/L = 0.80,\ \delta = 35^{\circ}$ (b) $\lambda/L = 1.00,\ \delta = 35^{\circ}$ (c) $\lambda/L = 1.20,\ \delta = 35^{\circ}$

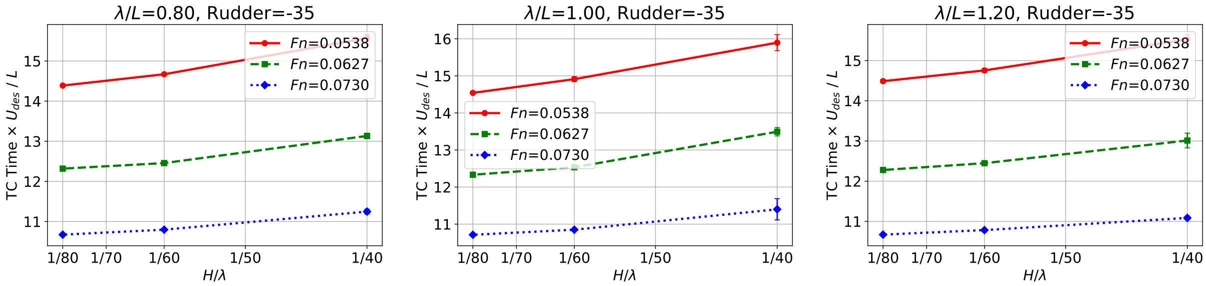

(d) $\lambda/L = 0.80,\ \delta = -35^{\circ}$ (e) $\lambda/L = 1.00,\ \delta = -35^{\circ}$ (f) $\lambda/L = 1.20,\ \delta = -35^{\circ}$

Figure 23: Variation of time to complete one turn (obtained from the fit) with wave slope (The vertical bars at each data point represent the 95% confidence interval of the reported mean value). Solid line indicates 600 RPM, dashed line indicates 700 RPM and dotted line indicates 800 RPM

and rudder angles. Thus the increased drift observed in Figure 20 is contributed by both increase in drift velocity and increase in time to complete one turn.

3.2.4. Variation with wavelength

Figure 24 shows the variation of relative drift direction with wavelength for different combinations of propeller speeds, wave slopes and rudder angles. It can be seen that the relative drift direction is marginally higher at $\lambda/L = 1.00$ as compared to other wavelengths. This trend is observed for most combinations of wave slopes, forward speeds and rudder angles. However, a few cases also exhibit a higher relative drift direction at $\lambda/L = 1.20$ as compared to $\lambda/L = 1.00$. Thus the relative drift direction is maximum at $\lambda/L = 1.00$ and decreases with both lower and higher wavelengths. This observation is in line with the experimental study of [13]. However, the statistical significance of this trend is not very high as can be seen from the height of the confidence interval relative to the variations in the relative drift direction in Figure 24.

Figure 25 shows the variation of drift distance with wavelength for different combinations of propeller speeds, wave slopes and rudder angles. It can be seen that from $\lambda/L = 0.80$ to 1.00 the drift distance does not significantly change for all combinations of wave slopes, propeller speeds and rudder angles. However, from $\lambda/L = 1.00$ to 1.20 the drift distance shows a decrease across all cases except for propeller speed = 600 RPM, $H/\lambda = 1/80$ and $\delta = 35^{\circ}$. Thus at larger wavelength the drift distance is lower but this trend in not observed for $\lambda/L < 1.00$.

Figure 26 shows the variation of drift velocity with wavelength for different combinations of wave slopes, propeller speeds and rudder angles. It can be seen that the drift velocity decreases in most cases from $\lambda/L = 1.00$ to $\lambda/L = 1.20$. However, there is no significant trend in the variation of drift velocity with wavelength over $\lambda/L = 0.80$ to $\lambda/L = 1.00$.

Figure 27 shows the variation of radius of turn with wavelength for different combinations of wave slopes, propeller speeds and rudder angles. It can be seen that the radius of turn decreases with an increase in

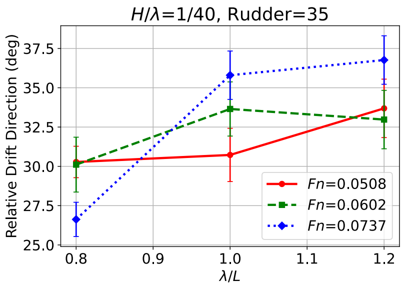

(a) $H/\lambda = 1/40,\ \delta = 35^{\circ}$

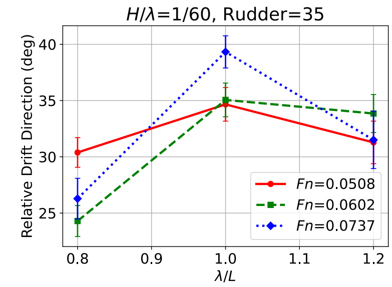

(b) $H/\lambda = 1/60,\ \delta = 35^{\circ}$

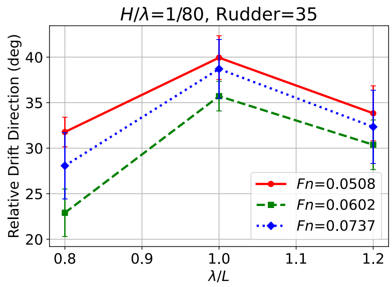

(c) $H/\lambda = 1/80,\ \delta = 35^{\circ}$

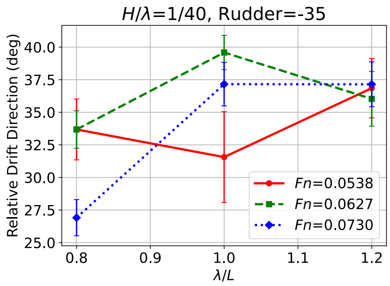

(d) $H/\lambda = 1/40,\ \delta = -35^{\circ}$

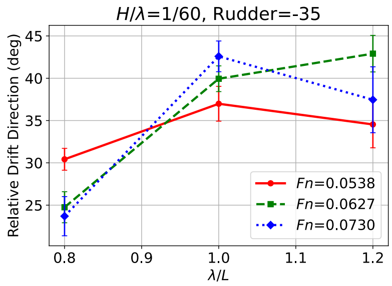

(e) $H/\lambda = 1/60,\ \delta = -35^{\circ}$

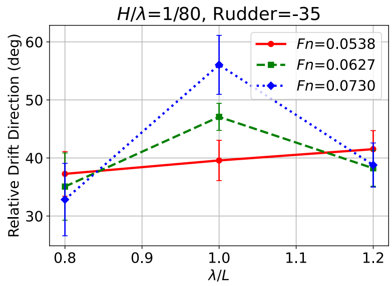

(f) $H/\lambda = 1/80,\ \delta = -35^{\circ}$

Figure 24: Variation of drift direction (obtained from the fit) with wavelength (The vertical bars at each data point represent the 95% confidence interval of the reported mean value). Solid line indicates 600 RPM, dashed line indicates 700 RPM and dotted line indicates 800 RPM

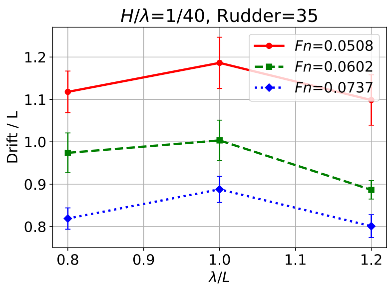

(a) $H/\lambda = 1/40,\ \delta = 35^{\circ}$

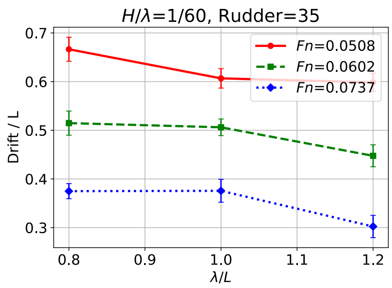

(b) $H/\lambda = 1/60,\ \delta = 35^{\circ}$

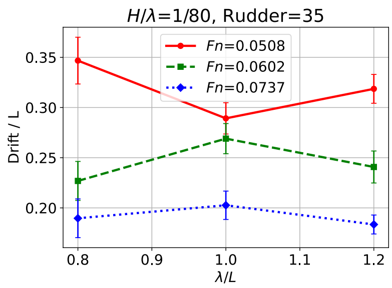

(c) $H/\lambda = 1/80,\ \delta = 35^{\circ}$

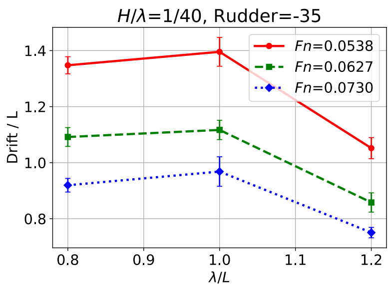

(d) $H/\lambda = 1/40,\ \delta = -35^{\circ}$

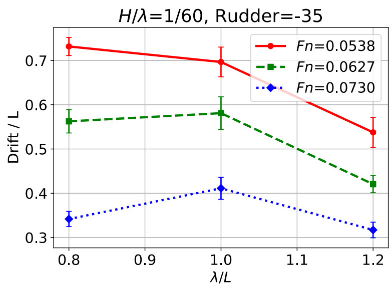

(e) $H/\lambda = 1/60,\ \delta = -35^{\circ}$

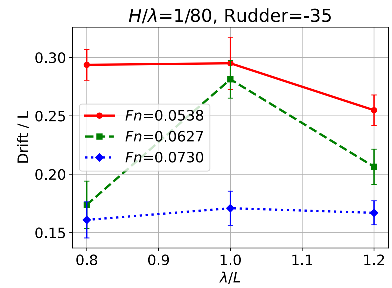

(f) $H/\lambda = 1/80,\ \delta = -35^{\circ}$

Figure 25: Variation of drift distance with wavelength (The vertical bars at each data point represent the 95% confidence interval of the reported mean value). Solid line indicates 600 RPM, dashed line indicates 700 RPM and dotted line indicates 800 RPM

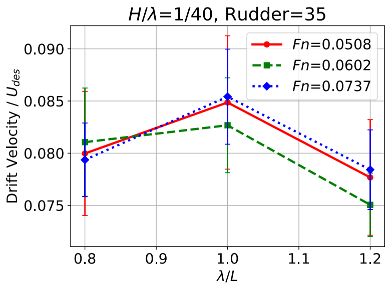

(a) $H/\lambda = 1/40,\ \delta = 35^{\circ}$

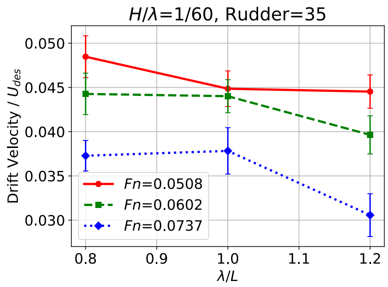

(b) $H/\lambda = 1/60,\ \delta = 35^{\circ}$

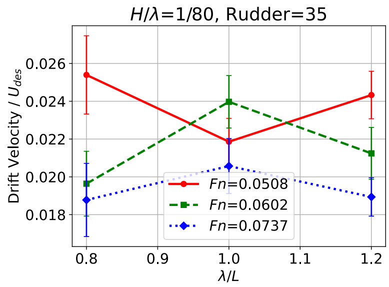

(c) $H/\lambda = 1/80,\ \delta = 35^{\circ}$

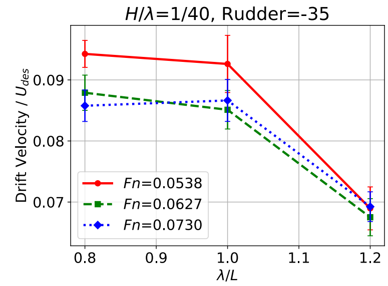

(d) $H/\lambda = 1/40,\ \delta = -35^{\circ}$

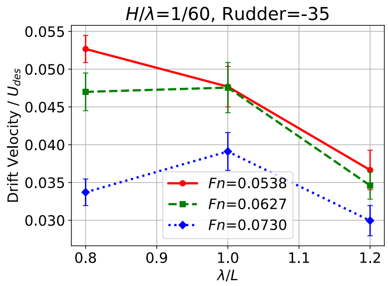

(e) $H/\lambda = 1/60,\ \delta = -35^{\circ}$

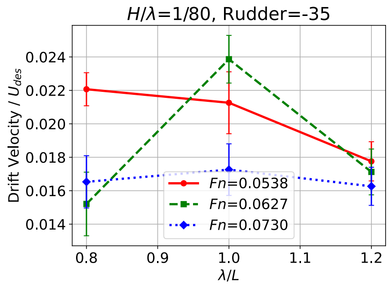

(f) $H/\lambda = 1/80,\ \delta = -35^{\circ}$

Figure 26: Variation of drift velocity (obtained from the fit) with wavelength (The vertical bars at each data point represent the 95% confidence interval of the reported mean value). Solid line indicates 600 RPM, dashed line indicates 700 RPM and dotted line indicates 800 RPM

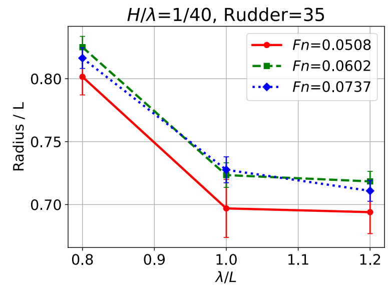

(a) $H/\lambda = 1/40,\ \delta = 35^{\circ}$

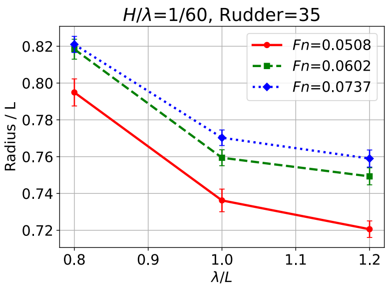

(b) $H/\lambda = 1/60,\ \delta = 35^{\circ}$

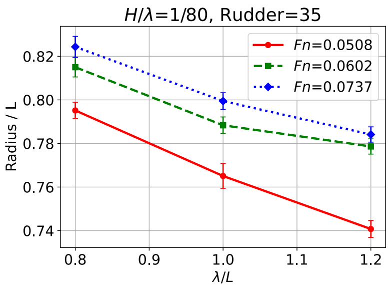

(c) $H/\lambda = 1/80,\ \delta = 35^{\circ}$

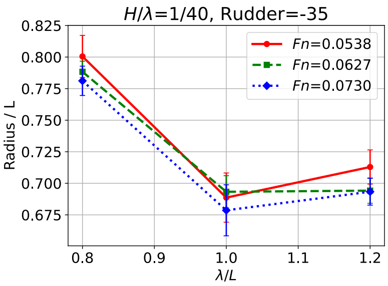

(d) $H/\lambda = 1/40,\ \delta = -35^{\circ}$

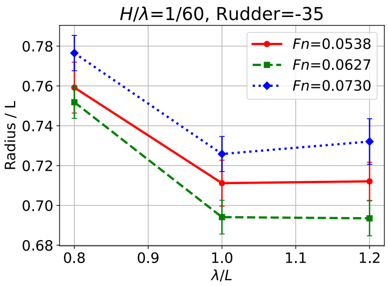

(e) $H/\lambda = 1/60,\ \delta = -35^{\circ}$

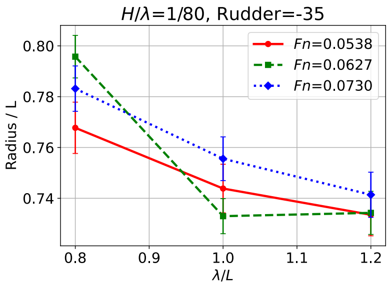

(f) $H/\lambda = 1/80,\ \delta = -35^{\circ}$

Figure 27: Variation of radius of turn (obtained from the fit) with wavelength (The vertical bars at each data point represent the 95% confidence interval of the reported mean value). Solid line indicates 600 RPM, dashed line indicates 700 RPM and dotted line indicates 800 RPM

wavelength from $\lambda/L = 0.80$ to $\lambda/L = 1.00$. However, from $\lambda/L = 1.00$ to $\lambda/L = 1.20$ the radius remains statistically same. Thus at lower wavelength the radius of turn is higher but at higher wavelength the radius of turn is almost same.

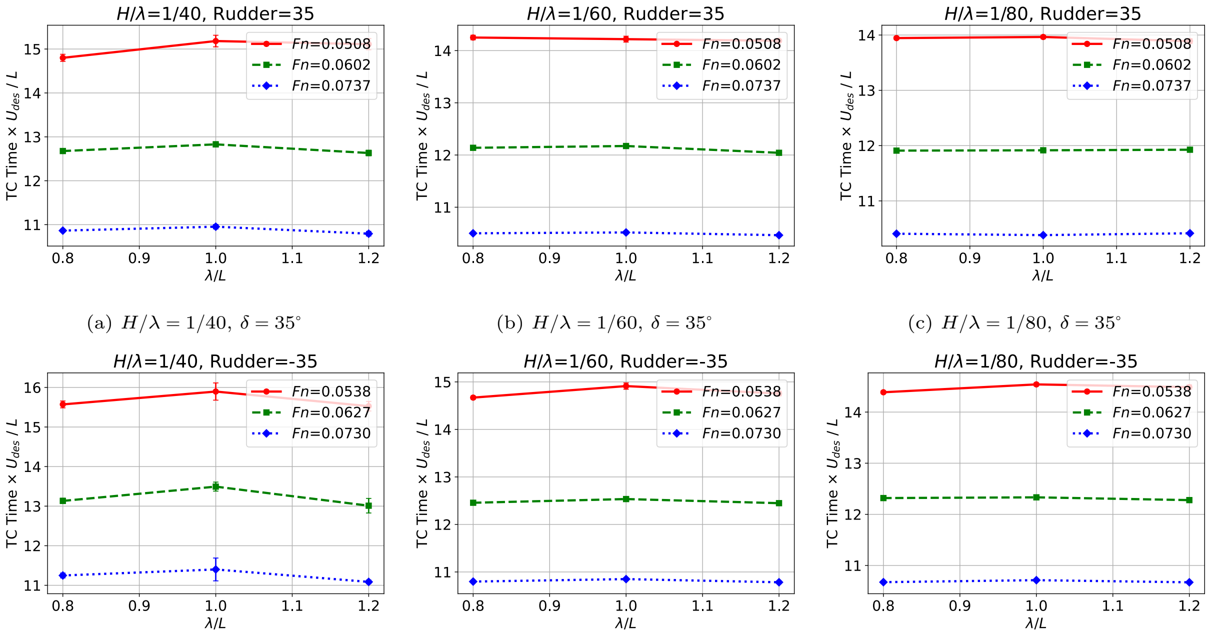

(a) $H/\lambda = 1/40$, $\delta = 35^\circ$ (b) $H/\lambda = 1/60$, $\delta = 35^\circ$ (c) $H/\lambda = 1/80$, $\delta = 35^\circ$

(d) $H/\lambda = 1/40$, $\delta = -35^\circ$ (e) $H/\lambda = 1/60$, $\delta = -35^\circ$ (f) $H/\lambda = 1/80$, $\delta = -35^\circ$

Figure 28: Variation of time to complete one turn (obtained from the fit) with wavelength (The vertical bars at each data point represent the 95% confidence interval of the reported mean value). Solid line indicates 600 RPM, dashed line indicates 700 RPM and dotted line indicates 800 RPM

Figure 28 shows the variation of time to complete one turn with wavelength for different combinations of wave slopes, propeller speeds and rudder angles. It can be seen that the time to complete one turn is independent of the wavelength and this trend is observed for all combinations of wave slopes, propeller speeds and rudder angles.

3.2.5. Summary of drift parameter variations

The drift direction exhibits consistent behavior across different experimental conditions. Starboard turns show a lesser relative drift direction compared to port turns, indicating marginal asymmetric drift characteristics between turning directions. Furthermore, the drift direction remains independent of both propeller speed and wave slope, suggesting that these parameters primarily affect the magnitude rather than the direction of drift. The maximum drift direction occurs at a wavelength-to-ship-length ratio of $\lambda/L = 1.00$, with values decreasing at both lower and higher wavelengths. This observation aligns with findings from previous experimental studies [13], providing validation for the current experimental methodology and results. However, the statistical significance of this trend is not very high.

The drift distance remains essentially independent of whether the vessel executes port or starboard turns, indicating symmetrical drift magnitude regardless of turning direction. Drift distance demonstrates a clear inverse relationship with forward speed of the vessel and a proportional relationship with wave slope. The drift distance is observed to be marginally dependent on wavelength with a decrease exhibited at higher wavelengths. However, the statistical significance of this trend is not very high.

The drift velocity shows no significant difference between port and starboard turns, indicating symmetrical behavior regardless of turning direction. The drift velocity does not vary significantly with the forward speed of the vessel. Drift velocity exhibits a linear proportional relationship with wave slope. Finally, the drift velocity shows no significant variation with wavelength, indicating that the wavelength parameter does not substantially influence the vessel's drift velocity characteristics. Thus the drift velocity is primarily dependent only on the wave height and hull geometry.

The radius of turn is observed to be marginally larger for starboard turns (due to rudder-propeller interactions) and independent of forward speed and wave slope. The radius of turn decreases with wavelength from $\lambda/L = 0.80$ to $\lambda/L = 1.00$, then remains constant.

Starboard turns complete faster than port turns. The time to complete one turn decreases with increasing forward speed. The time to complete one turn increases with wave slope, suggesting a proportional relationship with wave slope. Finally, the time to complete one turn is observed to be independent of wavelength.

3.3. Analysis of effect of higher wave slope

In order to better understand the effect of wave slope on the drift behavior, the results of the case of $H/\lambda = 1/40$, $\lambda/L = 1.0$, propeller speed of 700 RPM and $\delta = 35°$ are shown in Figure 29 and compared against the results of the case of $H/\lambda = 1/60$, $\lambda/L = 1.0$, propeller speed of 700 RPM and $\delta = 35°$ shown in Figure 5 and Figure 6.

It can be seen from Figure 29a that the drift distances are larger than for the case of $H/\lambda = 1/40$. Unlike Figure 5c, Figure 29b shows that the course angle crosses over the heading angle when the heading comes close to $0°$ (waves incident from port). This means that the drift velocity in the sway direction induced by the waves exceeds the steady sway velocity induced in the turn. This is also evident from Figure 29c and Figure 29d that show the drift angle and sway velocity crossing the zero level. Similarly on the diametrically opposite end, the drift angle magnitude exceeds $-35°$. It can be seen from Figure 29e that the total velocity is same as the steady velocity observed for the case of $H/\lambda = 1/60$ (Figure 6b) but the magnitude of the dip in total velocity is larger. As the wave slope increases, the drift velocity also increases and this causes considerable drag force on the hull when the drift velocity aligns with the sway direction of the vessel. This results in a greater speed loss at higher wave slopes.

One of the prominent differences in $H/\lambda = 1/40$ case as compared to $H/\lambda = 1/60$ is in the yaw rate. For $H/\lambda = 1/40$ the yaw rate exhibits strong dips as shown in Figure 29f. It can be seen from Figure 29c that the sharp reduction in yaw rate aligns with the times when the vessel experiences the maximum drift angle. Notice however, that for $H/\lambda = 1/60$ depicted in Figure 6e the dip in yaw rate is not as sharp as observed in Figure 29f. The larger wave slope causes a larger drift velocity and this causes the vessel to experience a larger drift angle when the drift velocity aligns with the sway direction of the vehicle. The sway hydrodynamic forces on the fore and aft of the vessel determine the yaw moment acting on the vehicle and hence we see a drop in yaw rate. This explains the proportional increase in time to complete one turn as the wave slope increases as observed in Figure 23.

3.4. Analysis of effect of lower speed

In order to better understand the effect of propeller speed on the drift behavior, the results of the case of $H/\lambda = 1/60$, $\lambda/L = 1.0$, propeller speed of 600 RPM and $\delta = 35°$ are shown in Figure 30 and compared against the results of the case of $H/\lambda = 1/60$, $\lambda/L = 1.0$, propeller speed of 700 RPM and $\delta = 35°$ shown in Figure 5 and Figure 6.

It can be seen that the total velocity as shown in Figure 30e is lower than the steady velocity observed for the case of propeller speed of 700 RPM (Figure 6b). This is expected as the propeller speed is lower. From Figure 30d it can be seen that the sway velocity has slightly increased and the surge velocity has decreased compared to the case of propeller speed of 700 RPM (Figure 6a). Therefore the magnitude of the drift angle has increased significantly as seen in Figure 30c.

Another prominent difference is observed in the yaw rate. The yaw rate exhibits strong dips as shown in Figure 30f. These effects were not observed in the case of propeller speed of 700 RPM (Figure 6e). This

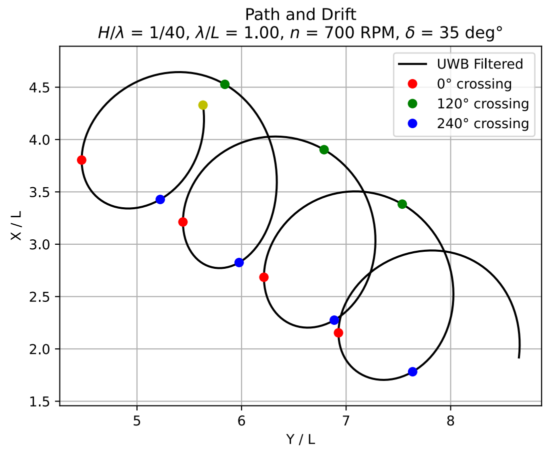

(a) Steady drift path

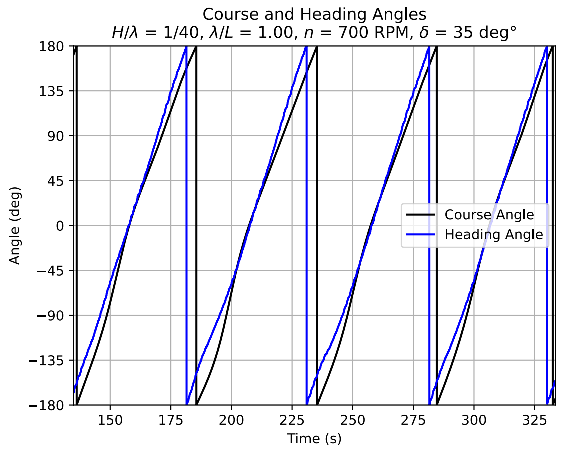

(b) Course and heading angles

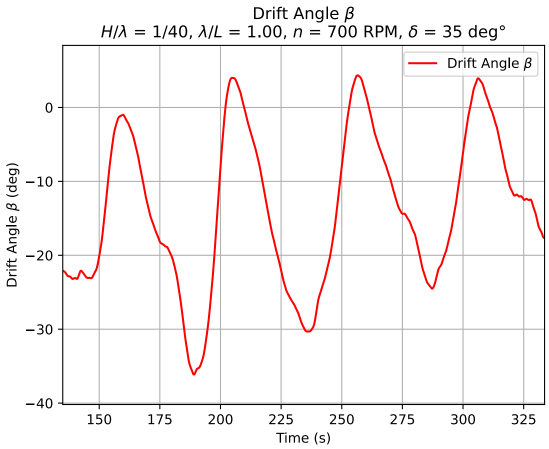

(c) Drift angle

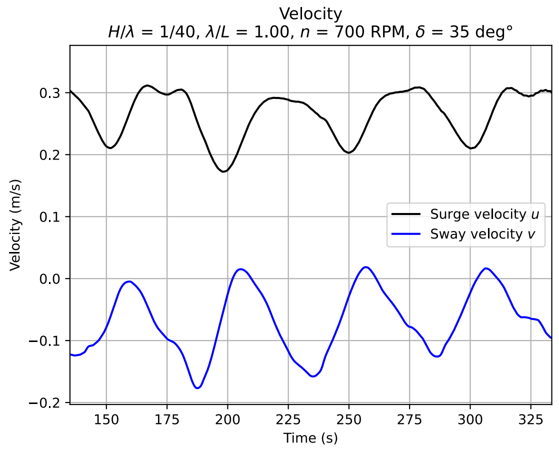

(d) Model scale velocity in BCS

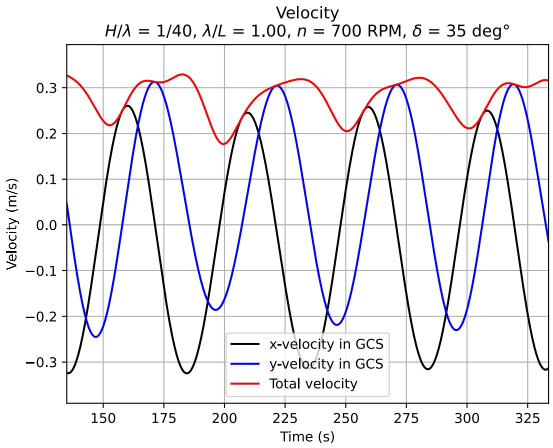

(e) Model scale velocity in GCS

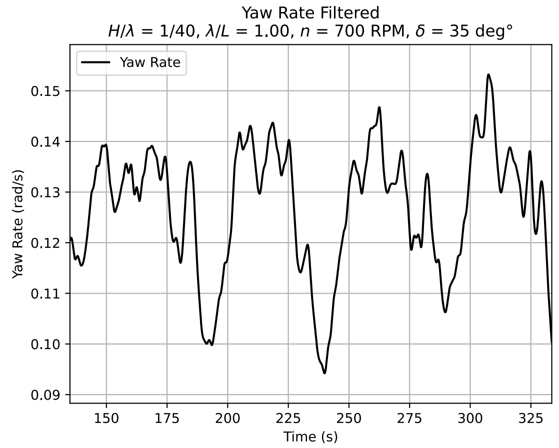

(f) Model scale yaw rate

Figure 29: Drift path, course, heading angle, drift angle, velocities and yaw rate for $\lambda/L = 1.0$, $H/\lambda = 1/40$, propeller speed of 700 RPM and rudder angle of $+35^{\circ}$

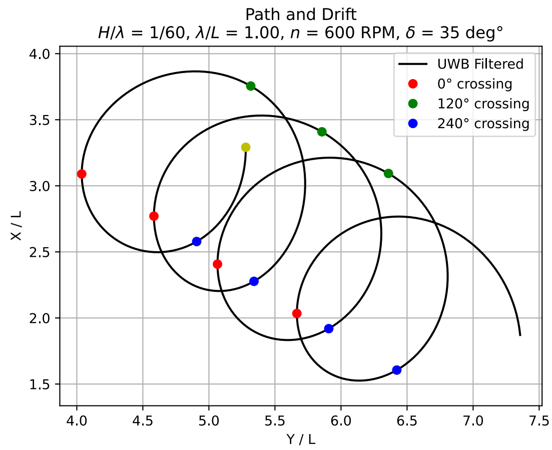

(a) Steady drift path

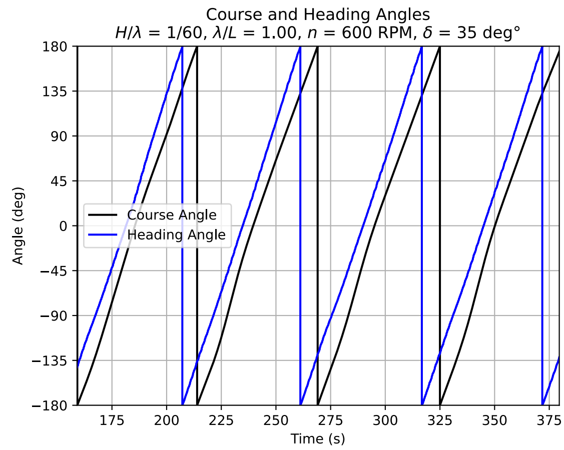

(b) Course and heading angles

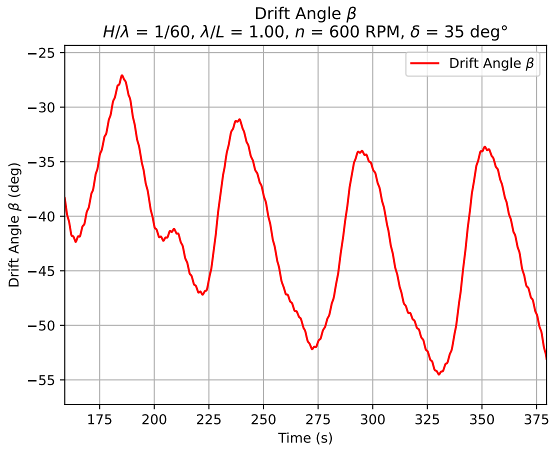

(c) Drift angle

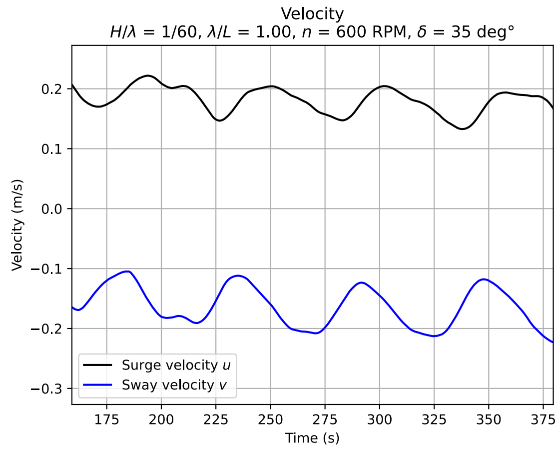

(d) Model scale velocity in BCS

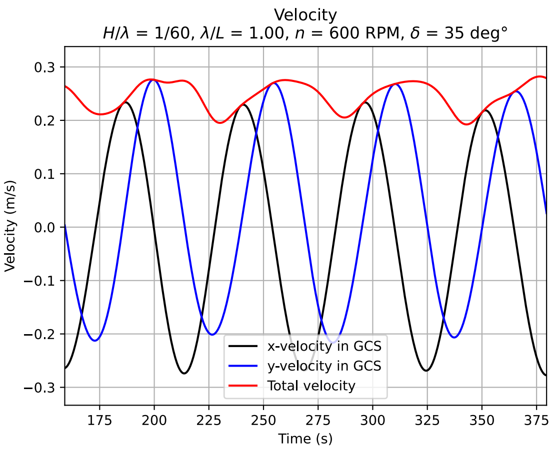

(e) Model scale velocity in GCS

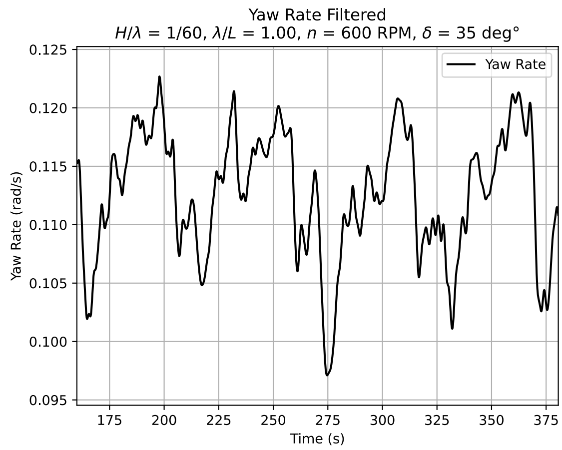

(f) Model scale yaw rate

Figure 30: Drift path, course, heading angle, drift angle, velocities and yaw rate for $\lambda/L = 1.0$, $H/\lambda = 1/60$, propeller speed of 600 RPM and rudder angle of $+35^{\circ}$

explains the increase in time to complete one turn as the propeller speed decreases as observed in Figure 18. The dip in yaw rate can be attributed to the same phenomenon as observed in the higher wave slope case. The larger sway velocity when the drift velocity is oriented along the sway direction of the vessel, the yaw rate experiences a drop due to the generation of yaw moment from the sway hydrodynamic forces.

3.5. Analysis of effect of initial heading

Previous studies like Klamo and Lin [12] have reported a significant scatter in drift direction for different initial heading direction with respect to the waves. In order to understand this effect, the case of $H/\lambda = 1/60$, $\lambda/L = 1.0$, propeller speed of 700 RPM and $\delta = 35^\circ$ is considered. The drift paths for initial headings of -90°, 90° and 0° are shown in Figure 31. Note that the waves are generated in all cases after the vessel has completed two turns and thus each case has the vessel in a different initial orientation when the waves are generated. It can be seen that the average drift direction $\overline{\gamma}_d$ is not significantly different for the three cases. In addition the average drift distance $\overline{\Delta}_d$ is also not significantly different for the three cases. Thus the initial orientation and the phase of the wave do not affect the drift characteristics significantly. This further strengthens the conclusion that the observed drift is not a transient effect but a steady state phenomenon.

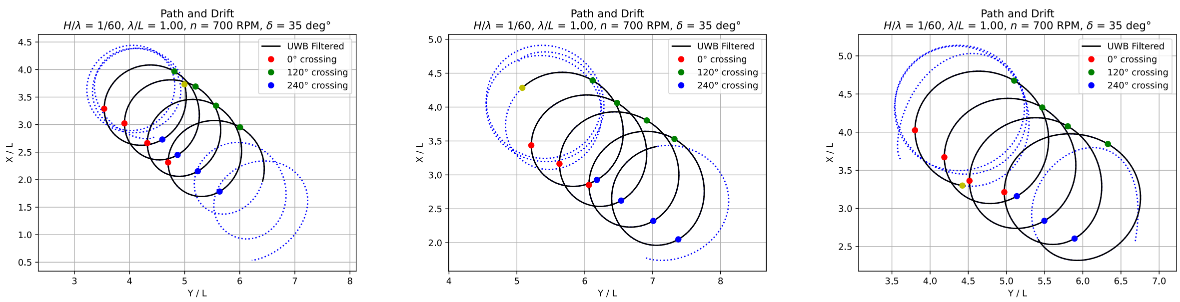

(a) $\psi_0 = -90^\circ$, $\overline{\Delta}_d = 0.498L$, $\overline{\gamma}_d = 32.49^\circ$ (b) $\psi_0 = 90^\circ$, $\overline{\Delta}_d = 0.485L$, $\overline{\gamma}_d = 26.29^\circ$ (c) $\psi_0 = 0^\circ$, $\overline{\Delta}_d = 0.488L$, $\overline{\gamma}_d = 27.73^\circ$

Figure 31: Effect of initial heading on drift behavior

4. Conclusion

This study presents a comprehensive experimental investigation of ship maneuvering in waves, addressing critical gaps in the existing literature through systematic repeatability testing and rigorous uncertainty quantification. The experimental campaign comprised of 270 turning circle tests across a full factorial design, exploring the combined effects of wave slope (1/80, 1/60, 1/40), wavelength-to-ship-length ratio (0.8, 1.0, 1.2), propeller speed, and rudder angle ($\pm 35^\circ$) on vessel drift behavior during turning maneuvers. The key findings are:

- Drift velocity increases linearly with wave slope. This linear trend of drift velocity has not been reported in the literature to our best knowledge and is significantly different from the quadratic variation with wave slope observed in drift forces and moments. Further theoretical analyses of ship-wave hydrodynamic interactions are needed to ascertain the physics causing the linear trend.
- The drift velocity is not affected by the hull's changing orientation relative to waves. However, the total velocity of the ship in turn decreases when the drift velocity is oriented along the sway direction of the vessel.
- Drift distance increases as propeller speed decreases. The increase arises from longer turning times at lower propeller speeds, while drift velocity itself remains nearly constant with forward speed. The turning times increase due to the significant drop in yaw rate when the drift velocity is aligned with the sway direction of the vessel and is more prominent at lower propeller speeds.
- Drift distance increases with wave slope due to a combination of increase in drift velocity and increase in time to complete one turn.

- Unlike calm water, where asymmetric turning radii are observed in port and starboard turns, the drift parameters (relative drift direction, drift distance and drift velocity) show no significant variation for port and starboard turns. This confirms that hull–wave interactions dominate the drift rather than the effect of propeller and rudder interaction with the waves.
- Maximum relative drift occurs at $\lambda/L = 1.0$ and the effect weakens at both shorter and longer wavelengths. However, the statistical significance of this effect is limited.
- The initial heading with respect to waves has negligible influence on drift direction.
- The maximum drift angle in a turn occurs when the drift velocity reinforces the sway velocity of the vessel in a turn. The maximum drift angle increases significantly as propeller speed decreases and wave slope increases. This further results in a greater drop in yaw rate.
- The dataset from this study provides a strong foundation for validating maneuvering models in waves, especially for low-powered vessels where safety in adverse seas is critical. These insights are relevant to the design and operation of modern ships subject to stringent emission and power constraints.

Future research will focus on developing theoretical frameworks that account for the transient nature of maneuvering in waves, explicitly incorporating time-dependence, encounter-frequency variation, and hull–wave hydrodynamic interactions during turning to explain the linear trend between drift velocity and wave slope and the drop in yaw rate during the maximum drift.

Acknowledgments

The authors would like to acknowledge the support from the Center of Excellence for Maritime Experiments to Maritime Experience (ME2ME), Department of Ocean Engineering, IIT Madras.

Appendix - A Tabulated Drift Data

The table below lists the drift parameters for different test conditions. Values are reported as mean ± 95% confidence interval. Column A denotes wave slope H/λ. Column B denotes λ/L. Column C denotes propeller speed in RPM. Column D denotes rudder angle in degrees. Column E denotes the non-dimensional drift distance $\overline{\Delta}_d$. Column F denotes relative drift direction $\overline{\gamma}_d$ in degrees. Column G denotes non-dimensional turn time (TC Time × U_{des}/L). Column H denotes non-dimensional radius (R/L). Column I denotes non-dimensional drift velocity (Drift velocity/U_{des}).

Source: Article Notebook

	A	B	C	D	E	F	G	H	I
0	1/40	0.8	600.0	-35.0	1.35 ± 0.03	33.7 ± 2.4	15.57 ± 0.09	0.800 ± 0.017	0.094 ± 0.002
1	1/40	0.8	600.0	35.0	1.12 ± 0.05	30.3 ± 1.0	14.80 ± 0.08	0.802 ± 0.015	0.080 ± 0.006
2	1/40	0.8	700.0	-35.0	1.09 ± 0.03	33.7 ± 1.5	13.13 ± 0.07	0.788 ± 0.009	0.088 ± 0.003
3	1/40	0.8	700.0	35.0	0.97 ± 0.05	30.1 ± 1.8	12.68 ± 0.04	0.825 ± 0.009	0.081 ± 0.005
4	1/40	0.8	800.0	-35.0	0.92 ± 0.02	26.9 ± 1.4	11.25 ± 0.06	0.781 ± 0.012	0.086 ± 0.003
5	1/40	0.8	800.0	35.0	0.82 ± 0.03	26.6 ± 1.1	10.86 ± 0.03	0.816 ± 0.008	0.079 ± 0.004
6	1/40	1.0	600.0	-35.0	1.40 ± 0.05	31.6 ± 3.6	15.90 ± 0.23	0.689 ± 0.020	0.093 ± 0.005
7	1/40	1.0	600.0	35.0	1.19 ± 0.06	30.7 ± 1.7	15.18 ± 0.13	0.697 ± 0.024	0.085 ± 0.007
8	1/40	1.0	700.0	-35.0	1.12 ± 0.04	39.6 ± 1.3	13.49 ± 0.12	0.693 ± 0.013	0.085 ± 0.003
9	1/40	1.0	700.0	35.0	1.00 ± 0.05	33.7 ± 1.7	12.83 ± 0.06	0.723 ± 0.010	0.083 ± 0.005
10	1/40	1.0	800.0	-35.0	0.97 ± 0.05	37.2 ± 1.7	11.40 ± 0.29	0.679 ± 0.020	0.087 ± 0.003
11	1/40	1.0	800.0	35.0	0.89 ± 0.03	35.8 ± 1.6	10.95 ± 0.05	0.728 ± 0.010	0.085 ± 0.005
12	1/40	1.2	600.0	-35.0	1.05 ± 0.04	36.9 ± 2.3	15.53 ± 0.12	0.713 ± 0.014	0.069 ± 0.004
13	1/40	1.2	600.0	35.0	1.10 ± 0.06	33.7 ± 1.9	15.11 ± 0.13	0.694 ± 0.017	0.078 ± 0.006
14	1/40	1.2	700.0	-35.0	0.86 ± 0.03	36.0 ± 2.1	13.01 ± 0.19	0.694 ± 0.010	0.068 ± 0.003

	A	B	C	D	E	F	G	H	I
15	1/40	1.2	700.0	35.0	0.89 ± 0.02	33.0 ± 1.9	12.63 ± 0.06	0.718 ± 0.008	0.075 ± 0.003
16	1/40	1.2	800.0	-35.0	0.75 ± 0.02	37.1 ± 1.7	11.09 ± 0.05	0.693 ± 0.011	0.069 ± 0.002
17	1/40	1.2	800.0	35.0	0.80 ± 0.03	36.8 ± 1.6	10.79 ± 0.05	0.711 ± 0.008	0.078 ± 0.004
18	1/60	0.8	600.0	-35.0	0.73 ± 0.02	30.4 ± 1.3	14.67 ± 0.03	0.759 ± 0.013	0.053 ± 0.002
19	1/60	0.8	600.0	35.0	0.67 ± 0.02	30.4 ± 1.3	14.25 ± 0.04	0.795 ± 0.007	0.048 ± 0.002
20	1/60	0.8	700.0	-35.0	0.56 ± 0.03	24.8 ± 1.9	12.46 ± 0.04	0.752 ± 0.008	0.047 ± 0.003
21	1/60	0.8	700.0	35.0	0.51 ± 0.03	24.3 ± 1.4	12.14 ± 0.03	0.818 ± 0.005	0.044 ± 0.002
22	1/60	0.8	800.0	-35.0	0.34 ± 0.02	23.7 ± 2.3	10.80 ± 0.02	0.777 ± 0.009	0.034 ± 0.002
23	1/60	0.8	800.0	35.0	0.37 ± 0.02	26.3 ± 1.8	10.50 ± 0.02	0.821 ± 0.004	0.037 ± 0.002
24	1/60	1.0	600.0	-35.0	0.70 ± 0.03	37.0 ± 2.1	14.91 ± 0.07	0.711 ± 0.012	0.048 ± 0.003
25	1/60	1.0	600.0	35.0	0.61 ± 0.02	34.7 ± 1.5	14.22 ± 0.06	0.736 ± 0.006	0.045 ± 0.002
26	1/60	1.0	700.0	-35.0	0.58 ± 0.04	39.9 ± 1.5	12.53 ± 0.04	0.694 ± 0.009	0.048 ± 0.003
27	1/60	1.0	700.0	35.0	0.51 ± 0.02	35.1 ± 1.5	12.17 ± 0.03	0.759 ± 0.004	0.044 ± 0.002
28	1/60	1.0	800.0	-35.0	0.41 ± 0.03	42.6 ± 1.8	10.85 ± 0.02	0.726 ± 0.009	0.039 ± 0.003
29	1/60	1.0	800.0	35.0	0.38 ± 0.02	39.3 ± 1.4	10.52 ± 0.03	0.770 ± 0.004	0.038 ± 0.003
30	1/60	1.2	600.0	-35.0	0.54 ± 0.03	34.5 ± 2.8	14.76 ± 0.05	0.712 ± 0.010	0.037 ± 0.003
31	1/60	1.2	600.0	35.0	0.60 ± 0.02	31.3 ± 1.9	14.19 ± 0.03	0.721 ± 0.005	0.045 ± 0.002
32	1/60	1.2	700.0	-35.0	0.42 ± 0.02	42.9 ± 2.2	12.45 ± 0.04	0.694 ± 0.009	0.035 ± 0.002
33	1/60	1.2	700.0	35.0	0.45 ± 0.02	33.8 ± 1.7	12.04 ± 0.03	0.749 ± 0.005	0.040 ± 0.002
34	1/60	1.2	800.0	-35.0	0.32 ± 0.02	37.5 ± 4.0	10.78 ± 0.03	0.732 ± 0.012	0.030 ± 0.002
35	1/60	1.2	800.0	35.0	0.30 ± 0.02	31.5 ± 2.6	10.46 ± 0.02	0.759 ± 0.005	0.031 ± 0.002
36	1/80	0.8	600.0	-35.0	0.29 ± 0.01	37.3 ± 3.9	14.39 ± 0.03	0.768 ± 0.010	0.022 ± 0.001
37	1/80	0.8	600.0	35.0	0.35 ± 0.02	31.8 ± 1.6	13.94 ± 0.03	0.795 ± 0.004	0.025 ± 0.002
38	1/80	0.8	700.0	-35.0	0.17 ± 0.02	35.1 ± 5.9	12.32 ± 0.03	0.796 ± 0.008	0.015 ± 0.002
39	1/80	0.8	700.0	35.0	0.23 ± 0.02	22.9 ± 2.6	11.91 ± 0.02	0.815 ± 0.005	0.020 ± 0.002
40	1/80	0.8	800.0	-35.0	0.16 ± 0.02	32.8 ± 6.3	10.67 ± 0.03	0.783 ± 0.009	0.017 ± 0.002
41	1/80	0.8	800.0	35.0	0.19 ± 0.02	28.1 ± 3.7	10.41 ± 0.03	0.824 ± 0.005	0.019 ± 0.002
42	1/80	1.0	600.0	-35.0	0.30 ± 0.02	39.6 ± 3.5	14.54 ± 0.03	0.744 ± 0.010	0.021 ± 0.002
43	1/80	1.0	600.0	35.0	0.29 ± 0.02	39.9 ± 2.4	13.96 ± 0.03	0.765 ± 0.006	0.022 ± 0.001
44	1/80	1.0	700.0	-35.0	0.28 ± 0.02	47.1 ± 2.4	12.33 ± 0.02	0.733 ± 0.007	0.024 ± 0.001
45	1/80	1.0	700.0	35.0	0.27 ± 0.02	35.7 ± 1.6	11.92 ± 0.02	0.788 ± 0.004	0.024 ± 0.001
46	1/80	1.0	800.0	-35.0	0.17 ± 0.01	56.0 ± 5.1	10.71 ± 0.02	0.756 ± 0.009	0.017 ± 0.002
47	1/80	1.0	800.0	35.0	0.20 ± 0.01	38.7 ± 3.3	10.38 ± 0.02	0.799 ± 0.004	0.021 ± 0.001
48	1/80	1.2	600.0	-35.0	0.25 ± 0.01	41.5 ± 3.2	14.49 ± 0.04	0.734 ± 0.008	0.018 ± 0.001
49	1/80	1.2	600.0	35.0	0.32 ± 0.01	33.8 ± 3.1	13.89 ± 0.04	0.741 ± 0.004	0.024 ± 0.001
50	1/80	1.2	700.0	-35.0	0.21 ± 0.02	38.2 ± 3.1	12.28 ± 0.02	0.734 ± 0.009	0.017 ± 0.001
51	1/80	1.2	700.0	35.0	0.24 ± 0.02	30.4 ± 2.8	11.93 ± 0.03	0.779 ± 0.004	0.021 ± 0.001
52	1/80	1.2	800.0	-35.0	0.17 ± 0.01	38.8 ± 3.8	10.67 ± 0.03	0.741 ± 0.009	0.016 ± 0.001
53	1/80	1.2	800.0	35.0	0.18 ± 0.01	32.3 ± 4.1	10.41 ± 0.02	0.784 ± 0.004	0.019 ± 0.001

Source: Article Notebook

References

[1] J. N. Newman, Marine Hydrodynamics, MIT Press, 1977.

[2] H. Maruo, The drift of floating objects due to waves and current, Journal of the Society of Naval Architects of Japan 1960 (108) (1960) 149–163.

[3] M. Hirano, J. Takashina, K. Takeshi, T. Saruta, Ship turning trajectory in regular waves, Transactions of the West-Japan Society of Naval Architects 60 (1980) 17–31.

[4] W. R. McCreight, Ship manoeuvring in waves, in: Proceedings of the 16th Symposium on Naval Hydrodynamics, 1986, pp. 456–469.

[5] ITTC, Session on the motions of the hull: Ship handling, in: Proceedings of the 16th International Towing Tank Conference (ITTC), Leningrad, USSR, 1981, chairman: Prof. Dr. S. Motora.

[6] M. Ueno, T. Nimura, H. Miyazaki, An experimental study on manoeuvring motion of a ship in waves, in: Proceedings of MARSIM'03, 2003, pp. RC–13–1–RC–13–7.
URL https://nippon.zaidan.info/seikabutsu/2003/00574/contents/0354.htm

[7] M. Ueno, T. Nimura, H. Miyazaki, K. Nonaka, Steady wave forces and moment acting on ships in manoeuvring motion in short waves, Journal of the Society of Naval Architects of Japan (188) (2000) 163–172.

[8] H. Yasukawa, N. Hirata, A. Matsumoto, et al., Evaluations of wave-induced steady forces and turning motion of a full hull ship in waves, Journal of Marine Science and Technology 24 (2019) 1–15. doi:10.1007/s00773-018-0537-3.
URL https://doi.org/10.1007/s00773-018-0537-3

[9] H. Yasukawa, et al., Study of ship turning in irregular waves, Journal of Marine Science and Technology 25 (4) (2020) 1024–1043.

[10] R. Skejic, O. M. Faltinsen, A unified seakeeping and maneuvering analysis of ships in regular waves, Journal of Marine Science and Technology 13 (2008) 371–394. doi:10.1007/s00773-008-0025-2.
URL https://doi.org/10.1007/s00773-008-0025-2

[11] H. Yasukawa, N. Hirata, Analysis of ship trajectory during periodically steady turning in waves, Ocean Engineering 286 (2023) 115581.

[12] J. T. Klamo, R. Lin, Analysis of experimental data from ship trajectories of turning circles in a regular seaway, in: Proceedings of the ASME 2010 International Mechanical Engineering Congress and Exposition, Vol. 11, ASME, Vancouver, British Columbia, Canada, 2010, pp. 89–98. doi:10.1115/IMECE2010-37664.
URL https://doi.org/10.1115/IMECE2010-37664

[13] D. J. Kim, K. Yun, J.-Y. Park, D. J. Yeo, Y. G. Kim, Experimental investigation on turning characteristics of kvlcc2 tanker in regular waves, Ocean Engineering 175 (2019) 197–206.

[14] H. Kim, et al., Initial and steady turning characteristics of kcs in regular waves, Journal of Marine Science and Technology 25 (4) (2020) 986–1002.

[15] Y. Sanada, H. Elshiekh, Y. Toda, et al., Onr tumblehome course keeping and maneuvering in calm water and waves, Journal of Marine Science and Technology 24 (2019) 948–967. doi:10.1007/s00773-018-0598-3.
URL https://doi.org/10.1007/s00773-018-0598-3

[16] O. el Moctar, F. Sprenger, T. E. Schellin, A. Papanikolaou, Numerical and experimental investigations of ship maneuvers in waves, in: Proceedings of the ASME 2016 35th International Conference on Ocean, Offshore and Arctic Engineering, Vol. 2, ASME, Busan, South Korea, 2016, p. V002T08A062. doi:10.1115/OMAE2016-54847.
URL https://doi.org/10.1115/OMAE2016-54847

[17] F. Sprenger, A. Maron, G. Delefortrie, T. van Zwijnsvoorde, A. Cura-Hochbaum, A. Lengwinat, A. Papanikolaou, Experimental studies on seakeeping and maneuverability of ships in adverse weather conditions, Journal of Ship Research 61 (3) (2017) 131–152. doi:10.5957/JOSR.170002.
URL https://doi.org/10.5957/JOSR.170002

[18] P. S., S. Rajendran, A unified seakeeping and manoeuvring model with a pid controller for path following of a kvlcc2 tanker in regular waves, Applied Ocean Research 116 (2021) 102860. doi:https://doi.org/10.1016/j.apor.2021.102860.
URL https://www.sciencedirect.com/science/article/pii/S014111872100331X

[19] A. Balagopalan, K. Tiwari, T. Rameesha, P. Krishnankutty, Manoeuvring prediction of a container ship using the numerical pmm test and experimental validation using the free running model test, Ships and Offshore Structures 15 (8) (2020) 852–865.

[20] Z. Xie, J. Falzarano, H. Wang, A framework of numerically evaluating a maneuvering vessel in waves., Journal of Marine Science & Engineering 8 (6) (2020).

[21] H. Yasukawa, Y. Yoshimura, Introduction of mmg standard method for ship maneuvering predictions, Journal of marine science and technology 20 (2015) 37–52.

[22] A. F. Molland, S. R. Turnock, D. A. Hudson, Ship resistance and propulsion, Cambridge university press, 2017.